Received: 2 October 2023 | Accepted: 15 August 2024

DOI: 10.1002/saj2.20765

Soil Science Society of America Journal

ORIGINAL ARTICLE

Fundamental Soil Science

Multimodal, microspectroscopic speciation of legacy phosphorus in two US Mid-Atlantic agricultural soils

Kathryn D. Szerlag[1] | **Matthew G. Siebecker**[2] | **Fatemeh Izaditame**[3] | **Paul Northrup**[4] | **Ryan Tappero**[5] | **Donald L. Sparks**[6]

[1]Department of Soil and Crop Science, Texas A&M University, College Station, Texas, USA

[2]Department of Plant and Soil Science, Texas Tech University, Lubbock, Texas, USA

[3]Department of Geosciences, University of Texas, Dallas, Texas, USA

[4]Department of Geosciences, Stony Brook University, Stony Brook, New York, USA

[5]National Synchrotron Light Source II, Brookhaven National Laboratory, Upton, New York, USA

[6]Department of Plant and Soil Science, University of Delaware, Newark, Delaware, USA

Correspondence
Kathryn D. Szerlag, Department of Soil and Crop Sciences, Texas A&M University, College Station, TX 77843, USA.
Email: kate.szerlag@ag.tamu.edu

Assigned to Associate Editor Owen Duckworth.

Funding information
USDA-NIFA, Grant/Award Number: 2017-67019-26333

Abstract

To understand phosphorus (P) mobility in agricultural soils and its potential environmental risk, it is essential to directly measure solid phase P speciation. Often, bulk P K-edge X-ray absorption near edge structure (XANES) spectroscopy followed by linear combination fitting (LCF) is utilized to determine the solid P phases in soil. However, this method may limit results to only a few major phases. Additionally, XANES spectra for different P species may have very similar features, leading to an over- or underestimate of their contribution to LCF. Here, an improved P speciation by pairing multimodal microbeam-X-ray fluorescence (μ-XRF) mapping coupled with μ-XANES (microbeam-X-ray absorption near edge structure) analysis to directly speciate major and minor P phases on the micron scale is provided. We combined maps of both tender (P, sulfur, aluminum, and silicon) and hard energy (calcium, iron [Fe], and manganese) elements to evaluate the elemental co-locations with P. To better account for uncertainty assigning XANES peaks to individual compounds, a more quantitative fingerprinting by "spectral feature analysis" was completed. With this analysis, an *R*-factor is reported for the fit. These results were compared to traditional LCF. Pre-edge fitting results revealed the presence of a two-component pre-edge feature for phosphate adsorbed to ferrihydrite. Additionally, phytate co-precipitated with ferrihydrite (Phytate-Fe-Cop) had a pre-edge feature, indicating direct association with Fe. Lastly, a unique P species associated with manganese oxide was identified in the soil via multimodal mapping and μ-XANES. These results allow for better prediction of P dissolution and mobility.

Abbreviations: μ-XANES, microbeam-X-ray absorption near edge structure; μ-XRF, microbeam-X-ray fluorescence; CEC, cation exchange capacity; EPA, Environmental Protection Agency; EXAFS, extended X-ray absorption fine structure; HMO, hydrous manganese oxide; LCF, linear combination fitting; NSLS-II, National Synchrotron Light Source II; OM, organic matter; SFA, spectral feature analysis; TES, tender energy spectroscopy; XAS, X-ray absorption spectroscopy; XFM, X-ray fluorescence microprobe.

1 | INTRODUCTION

Decades of poultry manure application to agricultural soils in excess of crop requirements in the US Mid-Atlantic region has led to a buildup of phosphorus (P) in these soils and is termed "legacy P" (Jarvie et al., 2013; Qin & Shober, 2018; Sharpley et al., 2011). This buildup of P has led to many of the soils in this region becoming a P source to the Chesapeake Bay, contributing to significant eutrophication problems (Boesch et al., 2001; Kleinman et al., 2011; McDowell et al., 2002; Qin & Shober, 2018). Furthermore, many of the soils with high amounts of legacy P in this region are predicted to be inundated with sea water as sea levels rise, a process that has already begun; this process will potentially release large amounts of legacy P into estuaries, exacerbating eutrophication in the Chesapeake Bay (Tully, Gedan, et al., 2019 et al., 2019; Tully, Weissman, et al., 2019). Therefore, it is crucial to understand the P speciation in these soils as the types of P present dictate P solubility, mobility, and environmental fate.

X-ray absorption spectroscopy (XAS) can speciate P in complex systems, like biosolids and manures (Peak et al., 2002; Shober et al., 2006; Zhang et al., 2022). Advances in tender energy XAS, and specifically X-ray absorption near edge structure (XANES) spectroscopy, have led to the use of bulk P K-edge XANES as the preferred method of in situ investigation of soil P speciation (Beauchemin et al., 2003; Gu et al., 2020; Sato et al., 2005; Szerlag et al., 2022). However, bulk XANES analysis suffers from limitations in determining the actual chemical forms of P due to the complexity, heterogeneity, minute spectral differences, and the number of possible P species present in the soil. Additionally, there are spectral similarities in standards used to determine the chemical forms of P present in soil samples (Gustafsson et al., 2020).

Determining speciation through XANES and linear combination fitting (LCF) is restricted by data quality and the representative selection of standards for species in the sample (Beauchemin et al., 2002; Gustafsson et al., 2020). Since the bulk P K-edge XANES spectra represent a weighted average of all forms of P within a soil sample, only the dominant P species will be represented using LCF because the spectra for the less dominant phases (minor species) will not significantly contribute to the spectra (Beauchemin et al., 2003). Using more than three or four standards in the LCF (to account for minor species) can cause overfitting (Beauchemin et al., 2003). These minor species contribute to overall P behavior in the soil; therefore, they are important to determine. However, bulk P K-edge XANES is not sensitive enough to determine all solid phase P species in a soil sample and may fail to accurately define P behavior in complex soil systems.

Although the primary peak position (i.e., the peak of the white line) for species of P in the tetrahedral PO_4 structure, where P has an oxidation state of plus five, is similar, the spectra contain secondary features that are indicative of different ligands and minerals bound to the phosphate group (Brandes et al., 2007), such as iron and manganese oxides (Ingall et al., 2011). Additionally, Brandes et al. (2007) also found that within the broad groups of P species, minute spectral differences still occurred, making it possible to distinguish between similar species. For example, the distinct features of apatite-group minerals include a broadening on the post-edge side of the absorption peak that creates a "shoulder" like feature and two secondary peaks at higher energy (Brandes et al., 2007; Hesterberg et al., 1999; Ingall et al., 2011; Kruse & Leinweber, 2008; Peak et al., 2002; Toor et al., 2005, 2006). Brandes et al. (2007) found fluorapatite to have a post-edge shoulder at 2154.5 eV, while phosphate minerals containing oxidized Fe have a pre-edge feature at 2148 eV; however, reduced iron (Fe)-P species do not have this feature. Hesterberg et al. (1999) also found that spectra for iron phosphate minerals have a unique pre-edge feature, and this feature decreases in intensity with decreasing mineral crystallinity.

Brandes et al. (2007) was one of the first to try to determine P speciation in an environmental sample using X-ray fluorescence spectromicroscopy, which utilizes both elemental spatial location imaging paired with P near-edge X-ray absorption fine structure spectroscopy (NEXFS, another name for XANES). The authors made XRF maps of a marine sediment with a submicron beam size at the scanning transmission X-ray microscope at the Advanced Photon Source to locate P regions of interest and possible elemental co-location with silicon (Si), aluminum (Al), magnesium, and sodium. They then used NEXFS to determine the P speciation at the locations of interest using a "fingerprinting" technique to analyze the spectra (Brandes et al., 2007). The "fingerprinting" technique uses peak location and presence/absence of pre-and

Core Ideas

- Coupling multimodal microbeam-X-ray fluorescence maps with μ-XANES (microbeam-X-ray absorption near edge structure) spectra aids in phosphorus species identification in soils.
- Fingerprinting by spectral feature analysis overcomes common problems of self-absorption in LCF of P μ-XANES.
- Phosphate adsorbed to ferrihydrite has a two-component pre-edge feature determined via spectral feature analysis.
- Phytate co-precipitated with ferrihydrite has a pre-edge feature and a peak shift to higher energy.
- A unique species of phosphorus associated with manganese oxide was identified via multimodal mapping and μ-XANES.

post-edge features of sample μ-XANES (microbeam-X-ray absorption near edge structure) compared to the same features in known standard spectra to determine the speciation of the sample spectra (Gamble et al., 2020). Several other researchers have been utilizing these microspectroscopic techniques to analyze soil P (Gamble et al., 2020; Hesterberg et al., 2017; Lombi et al., 2006; Schefe et al., 2011; Yamaguchi et al., 2021). Gamble et al. (2020) successfully utilized two beamlines to determine elemental co-location of P with Fe, Al, calcium (Ca), and Si in agricultural soils via μ-XRF (microbeam-X-ray fluorescence) maps of both tender and hard energy elements, followed by μ-XANES spectroscopy to determine P speciation.

Phosphorus speciation and spatial distribution were not assessed in our previous work (Szerlag et al., 2022), which primarily examined bulk speciation of P and macroscopic desorption experiments. Here, to address the knowledge gap of determining the minor P phases in soil, this research uses soil thin sections to determine both major and minor P phases by using a novel multimodal approach followed by a more quantitative fingerprinting method called fingerprinting by "spectral feature analysis" (SFA) of spectra for speciating legacy P in US Mid-Atlantic agricultural soils. Additionally, LCF of each μ-XANES was completed and compared to the fingerprinting by SFA results. The rationale to compare the fingerprinting by SFA technique to the LCF approach stems from the potential artifacts, particularly in micro-focused-XAS analysis of light elements such as phosphorus, that impact LCF fits. Such artifacts include particle size effects and self-absorption caused by increased elemental concentration at hotspots (Gamble et al., 2020). This work is multimodal in that it pairs advanced tender energy XAS data collected from the tender energy spectroscopy (TES) beamline 8-BM with the hard X-ray μ-XRF maps obtained from the 4-BM X-ray fluorescence microprobe (XFM) beamline, both at the National Synchrotron Light Source II (NSLS II). Coupling data collected from two different synchrotron beamlines enabled simultaneous evaluation of tender (P, sulfur [S], Al, and Si at TES) and hard energy (Ca, Fe, and manganese [Mn] at XFM) elements to identify the spatial distribution of legacy P, the elemental coordination, and P speciation at the micron-scale in two different agricultural soils from the US Mid-Atlantic region through micro-focused-XRF mapping and micro-focused-XANES analysis. Moreover, the high energy resolution and repeatability of the TES beamline enabled the identification of small changes (~0.1 eV) in spectral features resulting in a more complete picture of P speciation. Additionally, the energy-independent fixed nature of the beam position on the sample enables microbeam XAS of particles the same size as the probe beam, which enables P speciation of ~4 × 4 μm sized P hotspots (Northrup, 2019). We hypothesize that fingerprinting by SFA will better identify the chemical species of P in relation to its association with Al, S, Ca, Mn, and Fe verses conventional LCF and that SFA overcomes the common problem of self-absorption during LCF in P XANES.

2 | MATERIALS AND METHODS

2.1 | Sample preparation

Two composite soil samples with different physicochemical compositions were collected from agricultural fields (Ap horizon, 0- to 8-inch depth) in the US Mid-Atlantic region. Composite samples were collected manually with a soil sampling probe. Due to a long history of fertilizer and manure application, the soils are considered to have legacy P. After collection, the samples were air-dried and passed through a 2-mm sieve. The soils' physicochemical characteristics and the investigation of P mobility, or the amount of P that can be removed from the solid and become part of the soil pore water, were determined by Szerlag et al. (2022). Briefly, total elemental concentrations were determined via the EPA 3051 microwave-assisted acid digestion, where EPA is Environmental Protection Agency, and other parameters such as pH, organic matter (OM), cation exchange capacity (CEC), Mehlich III extractable nutrients, and texture were determined (Szerlag et al., 2022). The EPA 3051 is a microwave-assisted acid digestion protocol and is a standard method for digesting soils.

Soils with an excess of 700 mg kg^{-1} P were chosen for analysis using μ-XRF mapping and μ-XANES. For this work, the specific samples analyzed via micro-focused synchrotron techniques were at the edge of the field transect (EFT) and community garden Ap horizon (CGAp). A map of the sampling locations can be found in Szerlag et al. (2022). These samples represent sites with legacy P; EFT is the soil collected from an agricultural field with a corn–soybean rotation, while CGAp is soil obtained from a community garden, formally a dairy pasture (Szerlag et al., 2022). The air-dried soils were resin embedded, thin-sectioned (30 μm), and mounted on quartz slides. The thin sections were prepared by Spectrum Petrographics. Petrographic thin sections were double-sided polished specifically for the analysis of synchrotron based XRF. Additionally, they were processed for heat and oxygen sensitivity to prevent changes in oxidation state during fabrication. The quartz glass slide was a synthetic fused silica (Suprasil 2A). A diamond polish was used, and the resin was Epotek301. A cyanoacrylate-based adhesive (Krazy Glue) was used to mount the thin section to the quartz slide.

2.2 | Data collection

Beamline 8-BM (TES) at the NSLS II was used to map the P, Al, Si, and S microscale spatial distribution and for μ-XANES

collection at P hotspots of interest in the soil thin sections. Data collection for the tender energy μ-XRF mapping and μ-XANES was done in a helium environment using a germanium detector. The large μ-XRF maps were collected at 2700 eV using a 10 μm step-size, a 5 ms dwell time, and a 10 × 5 μm beam size. The large maps collected at TES were 2 × 2 mm in size. Smaller, higher resolution μ-XRF maps were then collected around areas of interest using a 4 × 4 μm beam size.

The TES beamline was also used for μ-XANES data collection at soil P hotspots of interest located on the tender energy μ-XRF map. Soil P hotspots of interest were chosen as spots with sufficient P intensity to yield acceptable μ-XANES spectra in terms of signal to noise and representative of different characteristics were chosen: large and small, high and low signal, diffuse and sharp, and with different elemental associations. At the P hotspots of interest on the TES map, P K-edge μ-XANES were collected using a 4 × 4 or 10 × 5 μm beam size to investigate the P bonding environment to determine the speciation at that location. The μ-XANES were collected in fluorescence mode over an energy range of 2140–2180 eV. For each hotspot, 40–100 scans were collected using on-the-fly continuous motion scanning. Scans were averaged together and normalized using the Athena software (Ravel & Newville, 2005). TES currently has an energy range of about 2.0–5.5 keV. This makes it impossible to investigate elemental co-location with Fe, Mn, and other higher Z elements.

The XFM beamline has an energy range of 2.1–21 keV. μ-XRF maps and XANES of the samples were also collected at beamline 4-BM (XFM) at NSLS II to correlate P with the higher Z elements. For each sample, the exact map location on the soil thin section that was mapped at the TES beamline was located and mapped at XFM. At XFM, μ-XRF maps included the Ca, Fe, and Mn elemental distribution in the soil thin section. The μ-XRF maps at XFM were collected using fluorescence mode at 12,700 eV with a 7 × 5 μm beam size and a 350 ms dwell time. The map sizes collected were roughly 2.2 × 2.2 mm.

2.3 | Data analysis

The IDL (Interactive Data Language) image-processing program was used to analyze the μ-XRF maps at TES. Larch GSE Map Viewer (Newville, 2013) was used to analyze the XFM μ-XRF maps. The two maps were then overlaid, and the elements co-located with P at P hotspots of interest were determined. To improve assessment of relevant standards for use in fingerprinting by SFA and LCF routines of the μ-XANES data, maps were viewed in the IDL and GSE MapViewer on a pixel-by-pixel basis to assess the correlations between P and other elements.

Edge normalization and background correction of μ-XANES spectra collected at TES were completed using Athena (Ravel & Newville, 2005). Spectra from known standards collected at TES (Figure S1) and bulk P K-edge XANES from Ingall et al. (2011) were used to compare collected μ-XANES spectra of the P hotspots to determine P speciation using distinct spectral features using a more quantitative fingerprinting method than found in Brandes et al. (2007) and Gamble et al. (2020) called fingerprinting by SFA. Please see Figure S2 for a flowchart outlining SFA. Pairing μ-XANES with the two μ-XRF maps illustrates the association of P with both tender (Al, Si, and S collected at TES) and hard (Ca, Mn, and Fe collected at XFM) energy elements. By using the μ-XRF maps, it is possible to assist in determining P speciation in ambiguous XANES spectra.

LCF was completed, and results were compared to the fingerprinting by SFA. Athena was used for LCF by fitting at most four standards. Reference spectra used in the fits were narrowed down based on the elemental co-locations determined from the μ-XRF maps. Goodness of fit was evaluated using the *R*-factor, uncertainties, and reduced chi-square values. The *F*-test (Hamilton Test) was used to compare the number of standards required to fit the data to determine if using three or four standards made a statistically significant difference (Calvin, 2013; Giannetta et al., 2020; Siebecker et al., 2017, 2018). To run the *F*-test, a regularized lower incomplete beta function calculator was used to determine if three or four standards should be included in the LCF (Soper, 2020). If the *F*-test had a value below 5%, then this indicated that four standards significantly improved the fit.

The fingerprinting technique is broadly a semiquantitative way to identify chemical speciation by matching characteristic pre-edge and post-edge features in a XANES spectrum to known features measured in reference standards. Fingerprinting of P K-edge XANES spectra has been used to qualitatively identify chemical species of P, particularly at the microscale (Brandes et al., 2007; Gamble et al., 2020). Here we employ fingerprinting by SFA, which is a more quantitative fingerprinting approach that deconstructs a given P XANES spectrum into its constituent features: the basic step-function of the absorption edge at the binding energy of the 1s electron, the primary peak resulting from a dominant electron transition, distinctive pre- and post-edge peaks related to other possible electron transitions involving bonding orbitals and neighboring atoms, and local structural resonances including extended X-ray absorption fine structure (EXAFS). For example, the main peak dominating phosphate XANES spectra (often called the "white line") results from a high-probability electron transition from P 1s to an available P 3p/O 2p molecular orbital (see e.g., Khare et al., 2007). The energy position of this peak is sensitive to the strength of external bonding to the phosphate O. For phosphate bonded to Fe(III), a pre-edge

feature is attributed to a lower probability transition from P 1s to an O 2p/Fe 4p orbital.

For implementation of SFA, the edge step is fit by an arctangent function; this and other features such as EXAFS oscillations resulting from reflection of the photoelectron from neighboring atoms are modeled as needed to provide accurate background for the critical diagnostic features. The main peak and any additional electronic transitions are fit by Gaussian functions. This approach was applied by Northrup et al. (2024) to Ca μ-XANES in order to differentiate between calcite, dolomite, ankerite, and apatite; to S μ-XANES to identify sulfide minerals and quantify mixtures of sulfide and sulfate; and to P μ-XANES to identify apatite.

The use of spectral feature analyses to fit microbeam P XANES data has some advantages over traditional LCF. Successful application of LCF requires appropriately matched reference spectra, which are not always available, and is particularly susceptible to experimental factors that impact peak heights. Self-absorption effects, concentration differences, particle size and orientation, and issues arising from background-subtraction and normalization of spectra, are more significant with microbeam measurements. LCF can give misleading results from nonideal data by fitting such discrepancies in peak heights and may not be sensitive to small, highly diagnostic features, like pre-edge features. In contrast, SFA decouples peak height from the more diagnostic peak position and enables independent measurement of small features. Preitzel et al. (2011) compared LCF analysis to a similar method of XANES SFA for bulk measurements of mixed S species. They concluded that LCF had advantages in quantifying mixtures of species when specific reference standards of appropriate low concentrations were measured; however, spectral deconstruction was more effective in categorizing and quantifying classes of S compounds when reference spectra exactly matching each component species were not available.

3 | RESULTS AND DISCUSSION

3.1 | Characterization of standards

Prior to analysis and discussion of sample spectra, it is important to discuss the XANES spectra of the standards to better understand the significance of spectral features, such as pre-edge peaks, post-edge shoulders, and the location, height, and shape of the main peak (white line). Standards collected at TES with a repeatable energy resolution of <0.1 eV (Figures S1 and S3) demonstrate the minute spectral differences, features, and trends found in different P species' XANES. Table 1 has a list of the standard abbreviations and standard descriptions used throughout this paper. Table 1 also includes a main peak (white line) position for all of the standards and sample points of interest (POIs) determined by using the centroid of the top portion of the main peak. Using the centroid of the top portion of the main peak, all standards and sample POIs were calibrated to Ingall et al. (2011) by setting the centroid of maximum intensity of fluorapatite to 2152.90 eV.

The high energy resolution and repeatability of the TES beamline allowed not only to determine peak shifts with more precision than previous beamlines, but it also allowed to see more detail in the XANES spectra. Table 2 describes key spectral details of the reference standards. It is important to note that the position of the white line varies slightly from Tables 1–2 as the position of the white line in Table 1 was determined by finding the centroid of the top portion of the main peak, while in Table 2, the position of the main peak was determined via SFA, which also takes into account the underlying edge-step. The positions of the main peaks reported in Table 2 are the positions used to describe the data throughout this paper. The benefits of the high energy resolution of TES is evident in the spectrum for phosphate adsorbed to ferrihydrite, which shows the pre-edge feature noted by Ingall et al. (2011) as characteristic of phosphate bonded to Fe(III); however, we further determined this to be a doublet of two peaks as discussed in Khare et al. (2007) (Table 2, Figure S4). In comparison, this doublet is larger in magnitude for phosphate coprecipitated with Fe(III) due to the increased number of Fe atoms bonded to each phosphate (Table 2, Figure S1). The pre-edge feature for P adsorbed to ferrihydrite being less intense than the pre-edge feature for the P coprecipitated with Fe corresponds with the findings of many studies (Brandes et al., 2007; Gamble et al., 2020; Hesterberg et al., 1999; Khare et al., 2004; Shober et al., 2006) that found the pre-edge features increase in intensity with increasing crystallinity. Meanwhile, the main 1s-3p peak is lower and broader in the coprecipitated sample. This is due to interactions between nearby phosphate ions in what may be referred to as a "particle size effect." As the number of phosphate ions in close proximity increases, that is, as particle size increases from isolated ions to molecular clusters or surface monolayers to nanoprecipitates to larger crystalline domains, the molecular orbital energy levels of nearby phosphate ions interact, which broadens and lowers the main peak (Figure S5).

The adsorbed species all have tall narrow main peaks, reflecting dispersed phosphate (isolated/monolayer phosphate; Figure 1, Figure S1). As described above, the height and shape of the main peak can be used to differentiate between adsorbed or crystalline phases as an adsorbed species has a stronger, taller main peak than the main peak of the crystalline species (Hesterberg et al., 1999; Figure S1). A peak shift was observed between P-Fe-Sorb (2153.47(1) eV) and P-Fe-Cop (2153.62(1) eV; Table 2, Figure 1). The more crystalline P-Fe-Cop standard has the highest amount of P-to-Fe bonds, and a spectrum with a well-developed pre-edge feature that closely matches the spectrum of strengite (Figure S3).

TABLE 1 White line peak locations of phosphorus μ-XANES (microbeam-X-ray absorption near edge structure) spectra for standards and P hotspots from two petrographic agricultural soil thin section μ-XRF (microbeam-X-ray fluorescence) maps (Figures 2 and 5).

Peak (eV)	Abbreviation of standards	Description of standards
2153.70	P-Fe-Cop	Phosphate co-precipitated with ferrihydrite
2153.45	P-Fe-Sorb	Phosphate adsorbed to ferrihydrite
2153.50	Phytate-Fe-Cop	Inositol hexaphosphate (phytate) co-precipitate with ferrihydrite
2152.70	Lipid-Fe-Cop	Phosphatidyl choline (lipid) co-precipitate with ferrihydrite
2153.61	P-HMO-Sorb	Phosphate adsorbed to hydrous manganese oxide
2153.50	P-Alumina-Sorb	Phosphate adsorbed to gamma alumina
2153.46	P-Boehmite-Sorb	Phosphate adsorbed to boehmite
2152.90	Fluorapatite	Fluorapatite [$Ca_5(PO_4)_3F$]
2153.48	Monetite	Monetite [$CaHPO_4$]
2153.02	ATP	Adenosine triphosphate (organic polyphosphate)
2153.26	Phytate	Inositol hexaphosphate (organic polyphosphate)
2152.88	Lipid	Phosphatidyl choline (organic polyphosphate)
EFT		
2153.56		EFT P1
2153.55		EFT P2
2153.56		EFT P3
2153.45		EFT P4
2153.56		EFT P5
CGAp slide		
2153.51		CGAp SM1 P1
2153.55		CGAp SM1 P2
2153.25		CGAp SM1 P3
2153.53		CGAp SM2 P1
2153.63		CGAp SM2 P2
2153.50		CGAp SM2 P3

Note: Both samples and standards were collected via micro-focused beam. The "white line" is the peak of the highest point in the absorption edge of XANES spectrum. The spectra for the standards are shown in Figure S1. These values were determined from the centroid position of the top of the peak of the white line, and slight variation in the peak positions in this table versus those in Table 2 determined through spectral analysis are normal because spectral feature analysis (SFA) also fits the edge step. All spectra in this table were calibrated to Ingall et al. (2011) by setting the centroid of the maximum intensity of the fluorapatite spectrum to 2152.90 eV.
Abbreviations: CGAp, community garden Ap horizon; EFT, edge of the field transect.

The main peaks for phosphate adsorbed to Al (both boehmite and gamma alumina) and P-Fe-Sorb are all at the same energy, 2153.46(1) eV, 2153.48(1), and 2153.47(1) eV, respectively (Table 2). The diagnostic difference between Al and Fe is that the Al standards show no pre-edge features (Table 2, Figure 1, and Figure S1). The relatively featureless spectra without a pre- or post-edge feature for the Al-P standards (P-Boehmite-Sorb and P-Alumina-Sorb) looks similar to the featureless spectra of the organic P (ATP, phytate, and lipid) standards (Figure 1), but they differ in peak location (Table 2; 2153.46(1) eV, 2153.48(1) eV vs. 2153.01(1) eV, 2153.14(2) eV, and 2152.93(1) eV, respectively) with the primary peak location of the Al-P species being up to 0.5 eV higher than the organic P standards. The peak for phosphate adsorbed to Mn is higher, 2153.60(1) eV (Table 2). Mn(III) association exhibits a pre-edge doublet similar to that for Fe(III), but the second of those peaks is at higher energy than that for Fe (Table 2).

The spectra from organic P standards have very specific peak positions that were tabulated in Table 2. Those positions are unique to specific organic P species and were used to identify organic P in the μ-XANES data. Additionally, the organic P species not associated with Fe lack pre- and post-edge features. One of the organic P species co-precipitated with Fe has a pre-edge feature and peak shift to lower energy compared to inorganic P co-precipitated with or adsorbed to Fe (Table 2, Figure 1). The peak positions for organic phosphates are all at lower energy than phosphate adsorbed to iron oxide (Table 2). In addition to the standards in Figure S1, three additional standards are presented in Figure S3 and are also included in Figure 1. These standards include two organic P standards (lipid co-precipitated with ferrihydrite [Lipid-Fe-Cop]

TABLE 2 Fitting results for the fingerprinting by spectral feature analysis (SFA).

Standard	Pre-edge 1 *E*, area	Pre-edge 2 *E*, area	Main peak *E*, area	Post-edge *E*, area	EXAFS main peak *E*	*R*
P-Fe-Cop	2148.53 (11) 0.18 (2)	2149.74 (5) 0.40 (2)	2153.62 6.20 (8)		2170.47	0.0004
P-Fe-Sorb	2148.56 (16) 0.17 (2)	2149.70 (17) 0.15 (2)	2153.47 (1) 9.25 (37)		2169.74	0.0006
Phytate-Fe-Cop	2148.53 0.14(1)	2149.74 0.368	2153.32 (3) 7.3(8)		2171.0 (1)	0.0003
Lipid-Fe-Cop			2152.70 (1) 8.06 (19)		2169.9 (1)	0.001
P-HMO-Sorb	2148.44 (23) 0.181 (18)	2150.40 (55) 0.071 (16)	2153.60 (1) 11.71 (5)		2169.18 (8)	0.0003
P-Alumina-Sorb			2153.48 (1) 10.11 (7)		2170.17	0.0004
P-Boehmite-Sorb			2153.46 (1) 10.47 (25)		2170.14	0.0003
Fluorapatite			2152.88 (1) 8.14 (13)	2155.6 3.31 (3)	2170.66 (8)	0.0005
Monetite			2153.26 (1) 5.42 (4)		2170.13 (9)	0.0004
ATP			2153.01 (1) 8.37 (15)		2169.96	0.0007
Phytate			2153.14 (2) 6.82 (21)		2169.5	0.0006
Lipid			2152.93 (1) 11.71 (10)		2168.20 (15)	0.0014
Sample						
EFT P1			2153.51 (1) 10.33 (6)		2169.99 (11)	0.0006
EFT P2	2148.56 0.077 (15)	2149.74 0.097 (15)	2153.51 (1) 9.68 (12)		2170.63 (9)	0.0004
EFT P3	2148.56 0.128 (14)	2149.74 Fe 0.137 (14) and 2150.4 0.049 (14)	2153.51 (1) 8.40 (8)		2169.74 (8)	0.0003
EFT P4			2153.27 (1) 7.20 (15)		2169.77 (6)	0.0002
EFT P5	2148.56 0.124 (11)	2149.74 0.136 (11) and Mn 2150.40 0.052 (11)	2153.51 (1) 8.26 (3)		2169.90 (7)	0.0002
CGAp SM1 P1	2148.56 0.07 (2)	2149.74 0.07 (2)	2153.49 (1) 9.06 (12)		2170.2 (1)	0.0005
CGAp SM1 P2	2148.56 0.09 (2)	2149.74 0.07 (2)	2153.53 (1) 9.70 (10)		2170.4 (4)	0.0005

(Continues)

TABLE 2 (Continued)

Standard	Pre-edge 1 *E*, area	Pre-edge 2 *E*, area	Main peak *E*, area	Post-edge *E*, area	EXAFS main peak *E*	*R*
CGAp SM1 P3		2152.45 (3) 0.798 (22)	2153.29 (1) 5.33 (13)	2155.28 (4) 0.73 (3)		0.0005
CGAp SM2 P1			2153.43 (1) 7.90 (11)		2171.20 (6)	0.0005
CGAp SM2 P2	2148.56 0.116 (16)	2149.74 0.090 (15) and Mn 2150.4 0.072 (16)	2153.58 (1) 10.49 (5)		2169.04 (8)	0.0003
CGAp SM2 P3	2148.56 0.078 (23)	2149.74 0.058 (22)	2153.50 (1) 10.67 (6)		2170.25 (11)	0.0007

Note: The results for the standards are on the top portion of the table and the sample spectra are on the bottom of the table. For each spectrum, first an arctangent was fit for the edge step. Then Gaussian curves for each spectral feature including the main peak (white line) pre-edge features, post-edge features, and EXAFS regions were fit. The table includes the top of the fitted Gaussian peak locations (eV) and the uncertainty for that location in parentheses after the peak location. Under each reported peak location is the peak area. An *R*-factor is also reported for the overall fit to the data.
Abbreviation: CGAp, community garden Ap horizon.

and phytate co-precipitated with ferrihydrite [Phytate-Fe-Cop]) as well as inorganic P co-precipitated with ferrihydrite (P-Fe-Cop). These co-precipitated standards are described in and synthesized by Santoro et al. (2019). We report the interaction of two organic P compounds with Fe, which is crucial to interpretation. It is important to note that while LCF analysis would require an exhaustive set of reference standards, SFA can identify these classes of organic P compounds (Prietzel et al., 2011). For phytate coprecipitated with Fe(III), the pre-edge doublet is less intense than for inorganic phosphate coprecipitated with Fe(III), indicating that there is less P–Fe interaction, but it is still higher than for phosphate adsorbed to iron oxide (Table 2, Figure 1, and Figures S1 and S3). This formation of the pre-edge feature was also observed in Prietzel et al. (2016). Notably, the main peak position for phytate coprecipitated with iron is shifted to higher energy than that of phytate without Fe, reflecting the influence of phosphate-Fe bonding (Table 2, Figure 1, and Figure S3). The emergence of a pre-edge feature and peak energy shift from the pure phytate standard to the Phytate-Fe-Cop standard (i.e., where P in phytate is directly bound to Fe) is significant because not including an energy-shifted Phytate-Fe-Cop component in LCF will result in underestimating the amount of organic P present in soils.

For lipid coprecipitated with Fe, there is no significant pre-edge feature (Table 1, Figure 1, and Figure S3), showing that this molecule's phosphate group is not bonded to Fe; any association of lipid with Fe is instead likely via carboxyl functional groups. This spectrum shows a dampened main peak height, likely due to a degree of self-absorption (Figure 1, Figure S3). Lastly, the apatite spectrum shows a lower main peak energy than even the organic phosphates, and a distinctive post-edge feature at 2155.6 eV (Table 2, Figure 1, and Figure S1). The apatite (i.e., fluorapatite) post-edge shoulder has been reported by many researchers (Brandes et al., 2007; Hesterberg et al., 1999; Ingall et al., 2011; Kruse & Leinweber, 2008; Peak et al., 2002; Toor et al., 2005, 2006).

3.2 | Fingerprinting by SFA versus LCF

The fingerprinting by SFA routine provides quantitative values in terms of peak location and peak area. These data are tabulated in Table 2. Importantly, an *R*-factor is also determined during the fingerprinting by SFA routine. This is the same type of calculated *R*-factor determined through LCF, but the fit is composed of a series of parameters such as gaussian peaks and an arctangent function for the edge step.

During the LCF fitting routine, often the white line peak intensity and position dominated the fits and did not allow for adequate representation of significant pre-edge features within the final fit. Additionally, often, solely the peak intensity (peak height) was the controlling factor for inclusion of specific standards, while the position of the white line was not well constrained. This essentially increased the contributions of standards with similar white line shape to the sample but may have different pre- and post-edge features. The strength of the fingerprinting technique, and specifically fingerprinting by SFA, allows for decoupling the influence of white line peak intensity from the presence of other diagnostic spectral features (i.e., pre-edge features and post-edge shoulders). This is a critical aspect and a strength of fingerprinting by SFA because LCF cannot adequately account for minor yet chemically relevant spectral features if the white line or peak

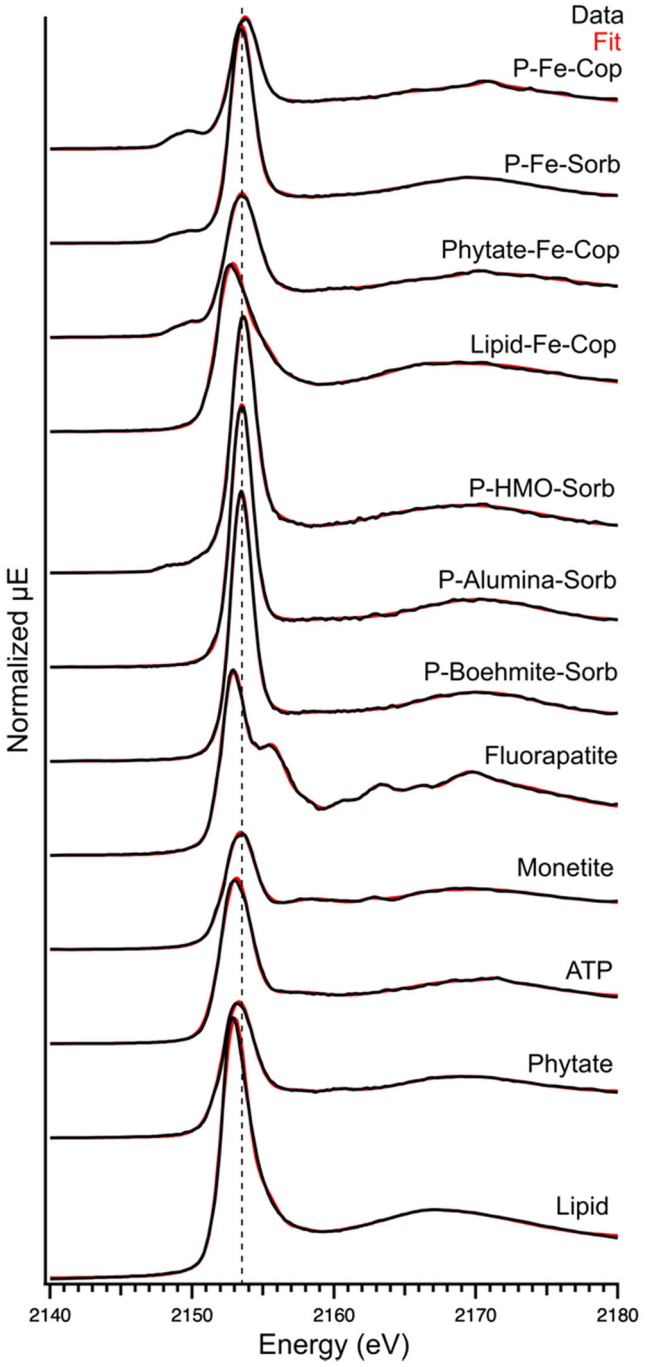

FIGURE 1 All standard spectra collected at beamline 8-BM, the tender energy spectroscopy (TES) beamline at the National Synchrotron Light Source II in black. Included in this figure are all of the fits (in red) for the spectral feature analysis (SFA) peak fitting routine used in the fingerprinting by SFA. To achieve this fit, first an arctangent is fit to the data for the edge-step. Next a series of Gaussian curves were fit to each spectral feature. The summation of all of these fitted curves yields the overall fit seen here in red. The spectral feature positions as well as the *R*-factor for the overall fits are reported in Table 2.

intensity is dominating the fit; this is especially relevant for data that may be suffering from the effects of particle size and/or self-absorption, which can be a common issue with fluorescence data and micro-focused fluorescence data (Gamble et al., 2020). By using the fingerprinting by SFA method, we can overcome the over reliance on peak intensity and focus on peak and shoulder positions beyond solely the white line.

3.3 | EFT, Crisfield, MD

The complete characterization of the soils used in this study can be found in Szerlag et al. (2022). In Szerlag et al. (2022), many soils were analyzed and two of those soils were chosen for further analysis to investigate in this study for their different physicochemical characteristics. Briefly, EFT was collected from an agricultural field with a corn, winter wheat, double-cropped soybean rotation in Crisfield, MD, in the Pocomoke Sound sub-watershed (Hydrologic Unit Code 02130201). EFT is a Queponco loam. This field has a long history of chicken litter application P in excess of crop need, leading to legacy P. This field site was chosen for its high soil-test P (303 mg kg^{-1} Mehlich III P, EPA 3051 total P 727 mg kg^{-1}) and proximity to the Chesapeake Bay with potential transport pathways for P export off the field via ditches connected to a stream. Delaware state law describes a soil with greater than 150 mg kg^{-1} Mehlich III P a high P soil (Shober & Sims, 2016). This soil also has a P saturation ratio of 76.9 and is therefore considered to be at very high risk for P loss (Szerlag et al., 2022).

The EFT soil has high soil test P values and therefore no longer receives P inputs. The EFT soil is a loam with 51% sand, 25% silt, and 24% clay. The pH of the soil is 5.4, OM content was determined to be 1.7%, and CEC is 10.4 $cmol_c$ kg $soil^{-1}$. Additionally, in Szerlag et al. (2022), different P pools in the soil were determined via a modified Hedley sequential extraction as well as bulk P K-edge XANES. The modified Hedley sequential extraction determined deionized water (DI) extractable P to be 5.2%, sodium bicarbonate extractible P to be 17.8%, sodium hydroxide extractable P to be 45.6%, hydrochloric acid extractible P to be 19.1%, and digest P to be 12.3% of total P. The bulk P K-edge XANES determined P speciation via LCF to be 21.2% Fe-P, 53.6% Al-P, and 25.2% to be Ca-P. For a full description of the methods used to determine the physicochemical characteristics, see Szerlag et al. (2022).

Although EFT is low in OM, the TES μ-XRF maps in Figure 2 indicate a large nebula-like shape in the lower portion of the map (Figure 2a) with elemental co-locations of P and S. The co-location of P and S is indicative of OM. Furthermore, in many soils, including those studied here, the dominant host for S is OM (see e.g., Xia et al., 1998). Additionally, we collected S K-edge μ-XANES at the same location as one of

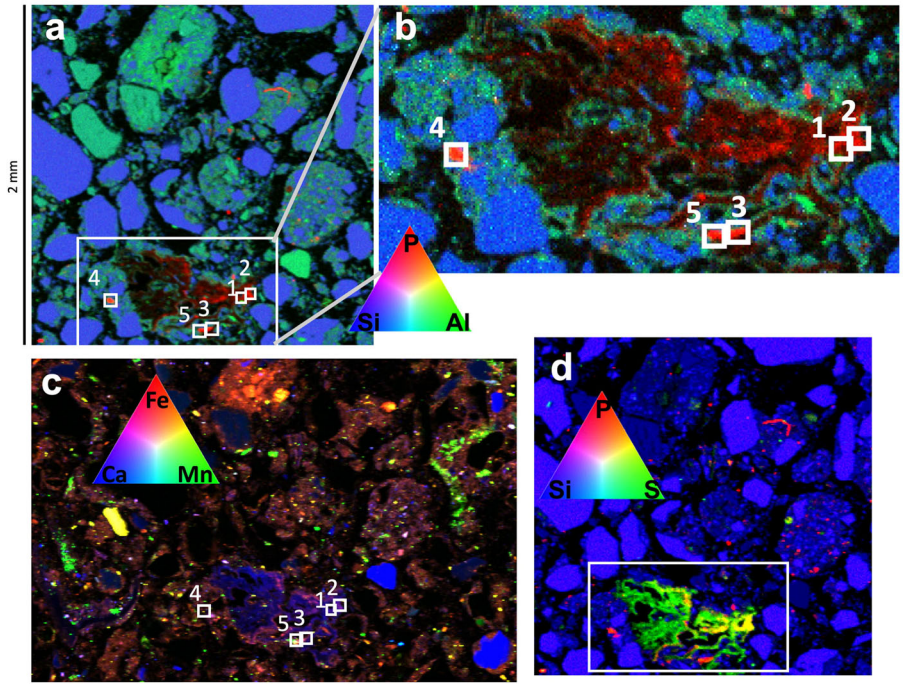

FIGURE 2 Sample edge of the field transect (EFT) (<2 mm) soil thin section; (a) a large 2 × 2 mm μ-XRF map collected at 8-BM (tender energy spectroscopy [TES]) using a 10 × 5 μm beam at 2700 eV. In panel (a), aluminum is in green; (b) a smaller μ-XRF (microbeam-X-ray fluorescence) map collected from within the larger map at beamline 8-BM (TES) using a 4 × 4 μm beam size at 2700 eV; (c) μ-XRF map collected at beamline 4-BM (X-ray fluorescence microprobe [XFM]) using a 7 × 5 μm beam size at 12,700 eV. Panel (c) is a map of the same location seen in panel (a); thus panel (a) is contained within panel (c). The two maps can be aligned, for example, using the distinct fluorescence morphology of pink and red colors in the amorphous regions in the lower part of the map. Panel (d) is the same mapping region as panel (a) except sulfur is in green. One of the distinguishing features common to all these maps is the unique morphology the organic matter enriched with phosphorus and sulfur that can be seen in each map. Calcium, Mn, and Fe can only be seen with XFM, thus confirming that the amorphous organic matter region was enriched in both Ca and Fe along with P and S. Furthermore, the specific location where μ-XANES (microbeam-X-ray absorption near edge structure) data were collected from this thin section are indicated with the numbered boxes 1–5. Those μ-XANES data are provided in Figure 3a.

the P POIs (EFT P2) (Figure S6). The S spectra indicate the presence of five different organic S species, sulfide/thiol, thiophene, sulfoxide, sulfonate, and sulfate (Figure S6; Einsiedl et al., 2007; Xia et al., 1998). This is typical of S XANES spectra of OM (Einsiedl et al., 2007; Xia et al., 1998). The P co-located with OM may be organic P species or may be associated with secondary Fe (hydr)oxides or clays that are also associated with OM. At the location of the nebula-like shape, a small, higher resolution map was collected at TES, and five μ-XANES spectra at the P K-edge were collected at POIs throughout this structure (Figures 2b and 3a).

All of the μ-XANES spectra are presented in Figure 3a. Figure 3b shows an overlay of EFT P1 and EFT P2 with iron and organic standards of interest identified during the fingerprinting by SFA routine. Figure 4a shows all of the μ-XANES spectra from both EFT and CGAp in black with the overall fit of the SFA used in the fingerprinting by SFA routine. The first point (i.e., P1) from which μ-XANES was collected has a tall, sharp peak that is indicative of adsorbed P; however, the lack of a pre-edge feature suggests that this is not P directly associated with Fe (Figure 3a,b) but it is associated with Al. The peak location (i.e., white line) of EFT P1 is 2153.51 eV, which is closest to P-Fe-Sorb (2153.47 eV), P-Boehmite-Sorb 2153.46 eV, and P-Alumina-Sorb is 2153.48 (Table 2). The fingerprinting by SFA overall fit has an *R*-factor of 0.0006 (Table 2).

Discerning this species requires elemental co-location information from both tender and hard energy μ-XRF maps (Figure 2a,c). At EFT P1, P was associated with S, Al, Ca, and Fe. The presence of S with P at this location indicates the presence of OM. The lack of Mn at P1 allows for exclusion of those species as possibilities. The presence of S, Al and Fe; lack of a pre-edge feature and post-edge shoulder; and main peak location close to P-Alumina-Sorb indicates that EFT P1 is P adsorbed to Al.

Interestingly, when including all of the standards in the LCF, the best LCF included an Mn-P. This standard was excluded because there was no Mn identified at this location on a pixel-by-pixel basis with color intensity and by examining the XRF spectrum at EFT P1. Therefore, P-HMO-Sorb, where HMO is hydrous manganese oxide, was excluded and LCF was completed again to get the best fit with standards

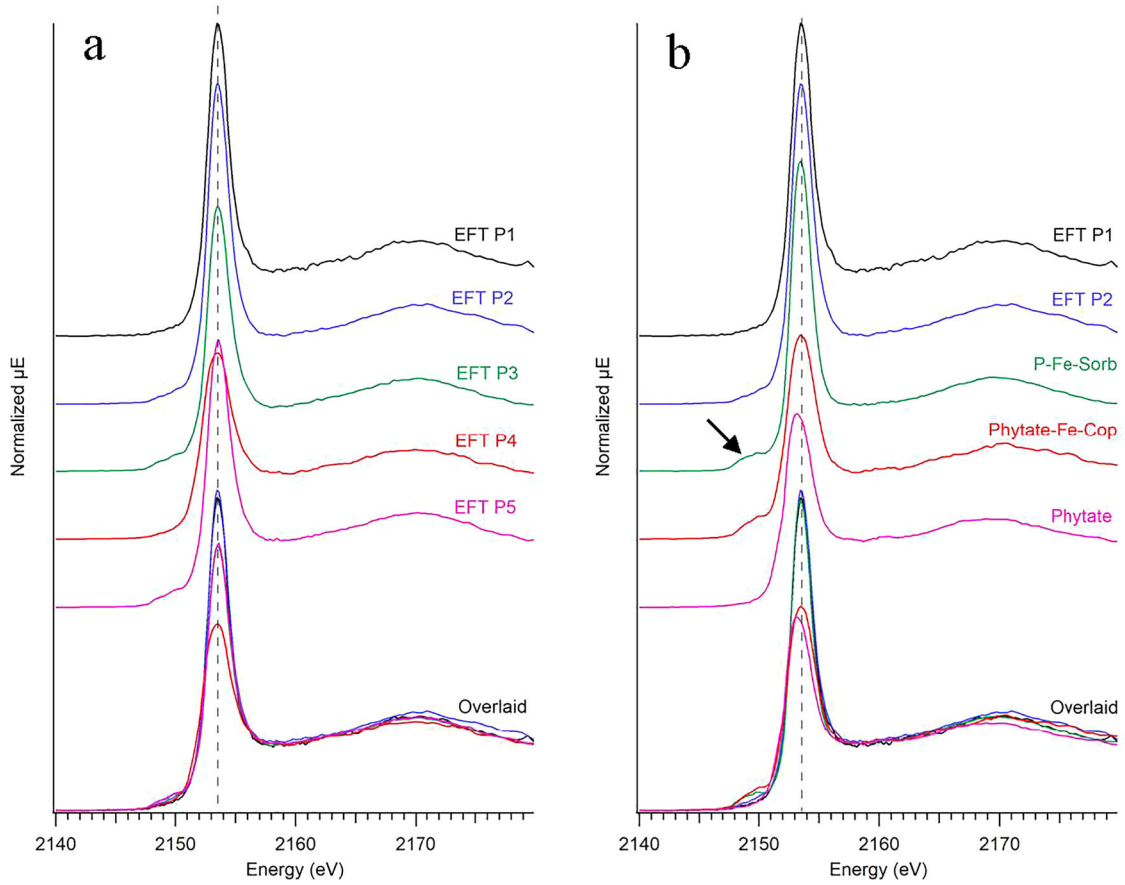

FIGURE 3 Phosphorus K-edge μ-XANES (microbeam-X-ray absorption near edge structure) from sample edge of the field transect (EFT). EFT is an agricultural soil, which was prepared as a petrographic thin section. (a) Each point (P1–P5) corresponds to the location labeled in Figure 2. Based on the multimodal maps shown in Figure 2, associations of elements at these locations can be used to assist in determining P speciation. These five spectra are plotted with two different techniques: stacked and overlaid. Both plotting techniques aid in identification of distinct spectral features, such as the pre-edge feature at ca. 2150 eV. (b) Phosphorus K-edge μ-XANES (P1 and P2) from sample EFT with three P standards ("P-Fe-Sorb" is P adsorbed to ferrihydrite, "Phytate-Fe-Cop" is phytate coprecipitated with ferrihydrite (Santoro et al., 2019), and "Phytate," which is a major component of organic P in soil). EFT is an agricultural soil, which was prepared as a petrographic thin section. P1 and P2 correspond to the location labeled in Figure 2. These five spectra are plotted in two different techniques: stacked and overlaid. Both plotting techniques aid in identification of distinct spectral features, such as the pre-edge feature at ca. 2150 eV. The three standards aid in the fingerprinting technique, which is used to identify P species in the soil. The arrow indicates the location of a pre-edge feature on an exemplary spectrum of a standard. Note the lack of pre-edge feature in EFT P1 indicating it is not associated with Fe.

from elements co-located with P at EFT P1. The LCF of EFT P1 determined this POI to be four different compounds: P-Fe-Cop 16.2%, P-Fe-Sorb 15.3%, P-Alumina-Sorb 61.6%, and Fluorapatite 9.9%, with an *R*-factor of 0.0037 (Table 3, Figure 4b). Note the lack of pre-edge feature and post-edge shoulder.

The spectrum for EFT P2 has a slight pre-edge feature (Figure 3b). The pre-edge indicates that there is P directly associated with Fe at EFT P2. The sharp, tall peak of EFT P2 indicates that this is adsorbed P. The peak location of EFT P2 is 2153.51 eV, which is identical to P1 and is closest to P-Fe-Sorb (2153.47 eV), 2153.46 eV for P-Boehmite-Sorb, and 2153.48 eV for P-Alumina-Sorb (Table 2). At EFT P2, P is co-located with S, Al, Ca, Mn, and Fe, which are the same elements co-located with P1, with the addition on Mn. The main peak position is close to P-Fe-Sorb and P-Alumina-Sorb, but too low for P-Fe-Cop or P-HMO-Sorb. The spectrum was fit with both Fe and Mn pre-edge features, however, and fit was better without including Mn in the SFA as there is no Mn contribution apparent at EFT P2. The pre-edge 1 (2148.56 eV) and pre-edge 2 (2149.70 eV) match P-Fe-Sorb, but at a reduced intensity. The overall fit using the peak fitting routine had an *R*-factor of 0.0004 (Table 2). Additionally, there is no post-edge as indicative of apatite, so there are no apatite species at this POI. Therefore, as determined through fingerprinting by SFA, EFT P2 is a mixture of P adsorbed to Fe and Al.

There was some disagreement between the fingerprinting by SFA and LCF. The LCF of EFT P2 determined that this POI was composed of P-Fe-Cop 23.9(1.2)%, P-HMO-Sorb

TABLE 3 Fitting results for linear combination fitting (LCF) of all P points of interest (POIs) in samples edge of the field transect (EFT) and community garden Ap horizon (CGAp) soils.

P speciation (%)	EFT P1	±	EFT P2	±	EFT P3	±	EFT P4	±	EFT P5	±	CGAp SM1P1	±	CGAp SM1P2	±	CGAp SM1P3	±	CGAp SM2P1	±	CGAp SM2P2	±	CGAp SM2P3	±
P-Fe-Cop	16.2	3.6	23.9	1.2	30.8	1.9			27.9	2.3	14.9	1.6	15.3	1.8					13.6	3		
P-Fe-Sorb	15.3	12.1																				
Phytate-Fe-Cop									27.1	2.4	34.4	1.6	10.5	1.8							21.9	0.9
Lipid-Fe-Cop																						
P-HMO-Sorb			39	2.1	49.6	0.6			32.8	2.1	10	1.5	36.7	1.7					67.6	0.9	36.2	1.9
P-Alumina-Sorb	61.6	8	31	1.9			7.4	1.1			41.1	1.4	36.3	1.6	3.5	1.8	39.5	1.4				
P-Boehmite-Sorb									10.5	1.9											42.2	1.7
Fluorapatite	9.9	1.4	7.7	0.7	10.1	0.8	16.8	2.3							11.7	3.3	10.6	2.1				
Monetite					6.2	2.2	47.3	4.8							49.6	4	49.4	3.4	13	2.9		
ATP															31.5	5.2						
Phytate							29.4	7.3														
Lipid																						
R-factor	0.0037		0.0013		0.0043		0.006		0.0019		0.0008		0.0009		0.021		0.01		0.0034		0.0012	
Reduced chi-square	0.0041		0.0014		0.0034		0.0034		0.0015		0.0007		0.0009		0.052		0.008		0.003		0.0014	

Note: The POIs names are along the top. The results in the table include the percentage of total P of the standard (along left side) with the uncertainties (±). *R*-factors and chi-square values are also reported along the bottom of the table and indicate the goodness of each fit for the LCF results.

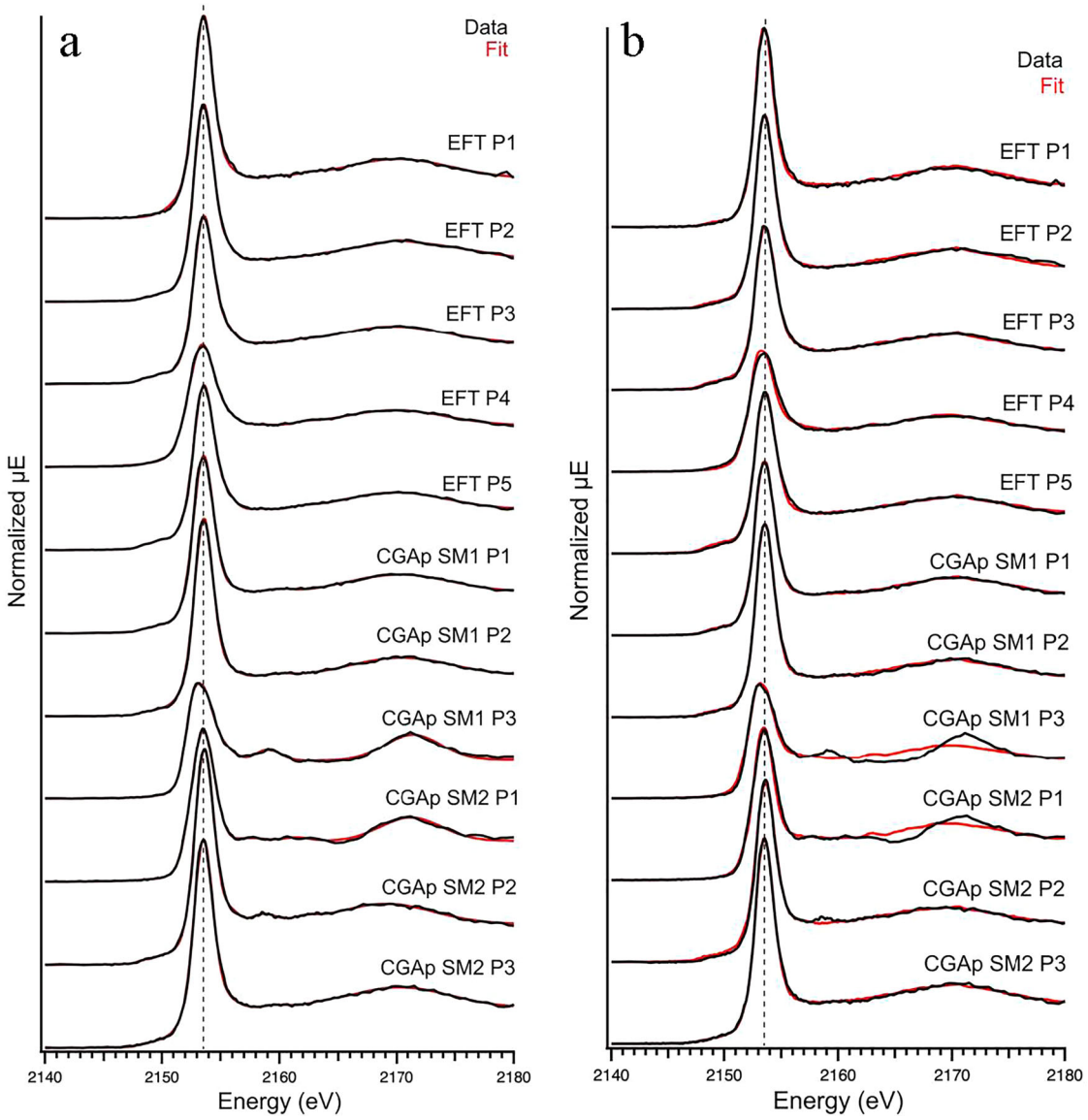

FIGURE 4 (a) Spectral feature analysis (SFA) of all sample P hotspot spectra from both edge of the field transect (EFT) and community garden Ap horizon (CGAp) collected at beamline 8-BM, the tender energy spectroscopy (TES) beamline at the National Synchrotron Light Source II in black. Included in this figure are all of the fits (in red) for the SFA peak fitting routine used in the fingerprinting by SFA. To achieve this fit, first an arctangent is fit to the data for the edge-step. Next a series of Gaussian curves were fit to each spectral feature. The summation of all of these fitted curves yields the overall fit seen here in red. The spectral feature positions as well as the *R*-factor for the overall fits are reported in Table 2. (b) Linear combination fitting (LCF) of all the sample micro-X-ray absorption near edge structure (µ-XANES) spectra from P points of interest in samples EFT and community garden Ap horizon (CGAp) in black with the LCF fits in red. Reference spectra used for the LCF of these points of interest (POIs) are in Figure S1. The complete list of reference spectra used in LCF of these spectra can be found in Table 3 along with the percentage P speciation, *R*-factor, and reduced chi-square for each.

39%, P-Alumina-Sorb (31%, and Fluorapatite 7.7%, with an *R*-factor of 0.0013 (Table 3, Figure 4b). Peak fitting as completed by the fingerprint by SFA ruled out both Mn and apatite species. This discrepancy shows that LCF has difficulty fitting minute spectral differences, especially for the pre-edge feature.

With an obvious pre-edge feature, both EFT P3 and EFT P5 appear to be P directly associated with Fe or Mn (Table 2, Figures 3a and 5, and Figure S7). Both have two clear components to the pre-edge, similar to the other Fe standards mentioned previously (P-Fe-Sorb, Phytate-Fe-Cop, P-Fe-Cop, and P-HMO-Sorb) (see Figure S4, Table 2, and Figure 4a for peak fitting results of pre-edge features). Again, the P3 and P5 spectra are indicative of adsorbed P given the tall, narrow peak. The main peak positions for EFT P3 and EFTP5 were both 2153.51 eV, which is close to that of P-Fe-Sorb (2153.47 eV) and a bit higher toward that of P-HMO-Sorb (2153.60 eV). The main pre-edge peaks for both

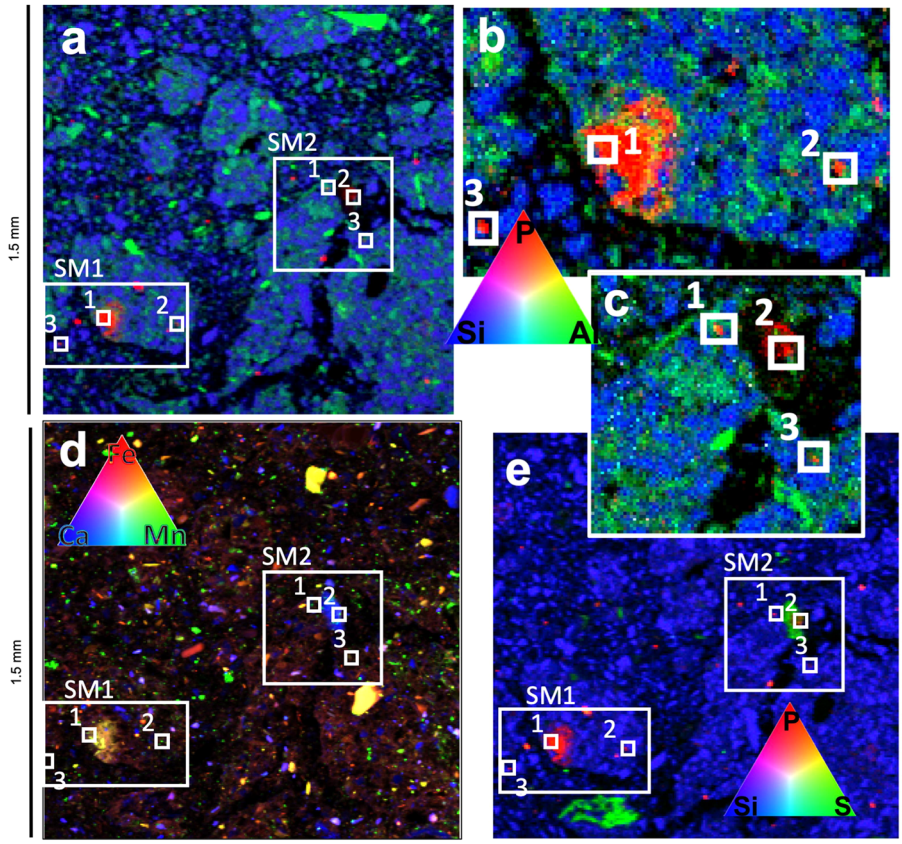

FIGURE 5 Sample community garden Ap horizon (CGAp) (<2 mm) soil thin section; (a) a large 1.5 × 1.5 mm μ-XRF (microbeam-X-ray fluorescence) map collected at 8-BM (tender energy spectroscopy [TES]) using a 10 × 5 μm beam at 2700 eV. In panel (a), aluminum is in green; (b) a smaller μ-XRF map (SM1) collected from within the larger map at beamline 8-BM (TES) using a 4 × 4 μm beam size at 2700 eV; (c) a smaller μ-XRF map (SM2) collected from within the larger map at beamline 8-BM (TES) using a 4 × 4 μm beam size at 2700 eV; (d) μ-XRF map collected at beamline 4-BM (X-ray fluorescence microprobe [XFM]) using a 7 × 5 μm beam size at 12,700 eV. Note that the locations for SM1 and SM2 are present in both panels (a) and (d), but (a) was collected at TES and (b) was collected at XFM. Panel (e) is the same mapping region as panel (a) except sulfur is in green. One of the distinguishing features to these maps is the unique presence of Fe and Mn co-located with P. This was only possible utilizing the multimodal approach. Furthermore, the specific location where μ-XANES (microbeam-X-ray absorption near edge structure) data were collected from this thin section are indicated with the numbered boxes SM1 P1, P2, P3 and SM2 P1, P2, P3. Those μ-XANES data are provided in Figure 6a.

EFT P3 and EFT P5 match P-Fe-Sorb with pre-edge 1 at 2148.56 eV and pre-edge 2 at 2149.70 eV. However, there is also some intensity matching the P-HMO-Sorb pre-edge peak (pre-edge 2 at 2150.4 eV) at both locations, but at a reduced intensity (Table 2). Including the Mn pre-edge peak fit improved the overall fit for the fingerprinting by SFA for both EFT P3 and EFT P5, and they had *R*-factors of 0.0003 and 0.0002, respectively (Table 2, Figure 4a). EFT P3 is co-located with S, Ca, Mn, and Fe, and EFT P5 is co-located with S, Al, Ca, Fe, and Mn (Figure 2b–d). Based on fingerprinting by SFA, both EFT P3 and EFT P5 are mixtures of P adsorbed to Fe and Mn.

The LCF of EFT P3 found the speciation to be P-Fe-Cop 30.8%, P-HMO-Sorb 49.6%, Fluorapatite 10.1, and Monetite 6.2% (Table 3, Figure 4b). The speciation of EFT P5 was determined to be P-Fe-Cop 27.9%, Phytate-Fe-Cop 27.1%, P-HMO-Sorb 32.8%, and P-Boehmite-Sorb 10.5% via LCF (Table 3, Figure 4b). Here, the LCF and fingerprint by SFA did not quite agree on the speciation as LCF identified the presence of Ca-P species in EFT P3 and an Al-P species in EFT P5, though both were in small amounts.

In contrast, EFT P4 does not have a pre-edge feature, so Fe and Mn species can be ruled out. EFT P4 has a peak location of 2153.27 eV and there is a noticeable 0.24 eV shift lower in energy from the other spectra (Table 2, Figure 4a, and Figure S8). This peak location more closely matches Phytate (2153.14 eV), P adsorbed to boehmite (2153.46 eV), P adsorbed to gamma alumina (2153.48 eV), and Phytate-Fe-Cop (2153.32 eV); however, in the absence of any pre-edge features, the contribution of P directly associated with Fe is unlikely. The short, wide peak suggests this is a precipitated rather than adsorbed species. Additionally, the spectrum without a pre-edge feature that shifted to lower energy may

indicate a region of organic P species adsorbed to Al or precipitated inorganic phosphate with Al. P4 is co-located with S, Al, Fe, and Mn. Given the co-location information, lack of a pre-edge feature, and peak shape, this location is primarily phytate adsorbed to Al or inorganic phosphate coprecipitated with Al.

The LCF of EFT P4 determined the speciation at this location to be P-Alumina-Sorb 7.4%, Fluorapatite 16.8%, Monetite 47.3%, and Phytate 29.4%, even though no post-edge feature was determined using peak fitting in the fingerprinting by SFA routine (Table 3, Figure 4b). Monetite was determined to be 47.3% in EFT P4 using LCF. This discrepancy may be due to the peak location being similar; however, no Ca was found to be co-located with P at EFT P4. However, both methods were in agreement for inorganic phosphate or phytate adsorbed to Al.

3.4 | CGAp, Newark, DE

The CGAp soil was collected from a community garden in Newark, DE, that used to be a dairy pasture and therefore has legacy P (Mehlich III extractible P of 199 mg kg^{-1}, EPA 3051 total P 937 mg kg^{-1}). The CGAp sample location was chosen because historically it was an agricultural field that received repeated manure applications in excess of crop need for many years. This led to a buildup of P in the soil, which is termed legacy P. This site is representative of what has historically occurred throughout the Delmarva peninsula on agricultural land. Due to CGAp's high soil test P values, it no longer receives P inputs. CGAp is an Elsinboro silt loam. The soil texture of CGAp is 13% sand, 65% silt, and 22% clay. The soil pH was 6.1, OM was determined to be 2.6%, and CEC was 7.1 $cmol_c$ kg $soil^{-1}$. The modified Hedley sequential extraction determined DI extractible P to be 3.5%, sodium bicarbonate extractible P to be 12.7%, sodium hydroxide extractible P to be 50.9%, hydrochloric acid extractible P to be 7.2%, and digest P to be 25.7% of total P. The bulk P K-edge XANES determined bulk P speciation to be 28.9% Fe-P, 58.3% Al-P, and 12.8% Ca-P. The sample was chosen for its unique physicochemical characteristics, as compared to EFT. The finer texture of this soil provides more surface area for adsorption of P. The topography of the site is flat, and the field location does not include a mode of transport off the field like a ditch, or stream flowing out of it and into a surface water body. For specific geographical site location, further physicochemical characterization of CGAp, and full description of specific methods used, see Szerlag et al. (2022).

The micro-focused data for CGAp are presented in Figure 5, which includes labels for each specific map. Although the large maps (Figure 5a, 5d, and 5e, collected with a 10 × 5 μm beam size) indicate many discrete P hotspots, two areas of interest (small maps Figure 5b and 5c) were selected to investigate with a finer beam size (4 × 4 μm) at lower energy, just above the P K-edge. Small map 1 (SM1, highlighted in Figure 5b) is P concentrated within a soil aggregate, where P is not co-located with S, but is rather co-located with both Fe and Mn (yellow color in Figure 5d) on the large map. This may be an indication of inorganic P species co-located with Fe. Small map 2 (SM2, highlighted in Figure 5c) is centered around distributed P hotspots on a larger particle enriched with S and Ca. Calcium was also identified on XFM in Figure 5d.

XANES spectra collected from specific spots on the maps in Figure 5 are shown in Figure 6a. CGAp SM1 P1 has a pre-edge feature that has two curves underneath that are at the same location as the P-Fe-Sorb standard but not the P-Fe-Cop or P-HMO-Sorb standards (Table 2, Figure 6a, and Figure S9). At 2153.49 eV (Table 2), the peak location of CGAp SM1 P1 is closer to P-Fe-Sorb (2153.47 eV), P-Alumina-Sorb (2153.48 eV), and P-Boehmite-Sorb (2153.46 eV), and is 0.13 eV lower than P-Fe-Cop. Additionally, the comparable peak width is similar to that of to P-Fe-Sorb, P-Alumina-Sorb, and P-Boehmite-Sorb, not suggesting that other components are present. The presence of organic P is not supported. CGAp SM1 P1 is an adsorbed species given the tall peak height. The pointed shape of CGAp SM1 P1 more closely matches P-Fe-Sorb and the peak intensity is greater than the more crystalline P-Fe-Cop standard (Figure S3). P is co-located with S, Al, Ca, Fe, and Mn. Although there was co-location with Ca in the μ-XRF map, there is no post-edge feature as for apatite. Additionally, the EXAFS main hump is comparable to P-Fe-Sorb and P-Alumina-Sorb. Taken together, these details are interpreted to show that CGAp SM1 P1 is a mixture of P-Fe-Sorb and P-Alumina-Sorb. More specifically, the pre-edge features are ~53% as intense as pure P-Fe-Sorb, indicating about 53% P-Fe-Sorb and 47% P-Alumina-Sorb (Table 2).

The LCF results determined the P speciation at CGAp SM1 P1 to be P-Fe-Cop 14.9%, Phytate-Fe-Cop 34.4%, P-HMO-Sorb 10%, and P-Alumina-Sorb 41.1% (Table 3). Although there is some agreement between the fingerprinting by SFA and LCF with including an iron phosphate standard and P-Alumina-Sorb, there are notable differences with the other species included in the LCF fit. First, the pre-edge doublet peaks match those in the iron phosphate standard, but there was no peak under the pre-edge region that matches the doublet for P-HMO-Sorb using the fingerprinting by SFA, so this species was ruled out by that method. The location of the main peak more closely matched P-Fe-Sorb and was too low for P-Fe-Cop. The LCF including P-Fe-Cop may be due to fitting the overall peak height instead of more diagnostic details such as peak position and pre-edge features for CGAp SM1 P1. The height of the main peak for CGAp SM1 P1 was 44% the height of the adsorbed phase. The last notable difference is that organic P was not supported at this location using the fingerprinting by SFA, yet Phytate-Fe-Cop was included

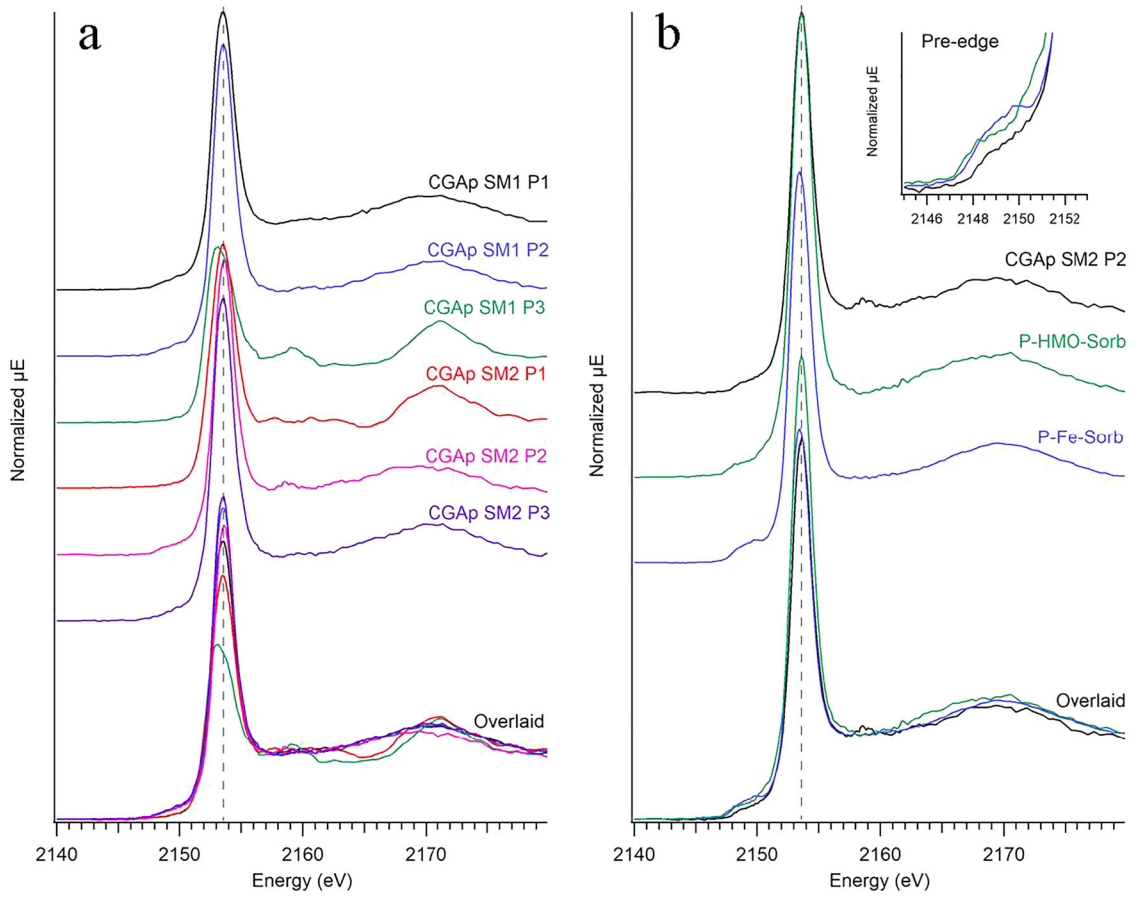

FIGURE 6 (a) Phosphorus K-edge µ-XANES (microbeam-X-ray absorption near edge structure) from sample community garden Ap horizon (CGAp). CGAp is an agricultural soil, which was prepared as a petrographic thin section. Each point (SM1 P1 through SM2 P3) corresponds to the location labeled in Figure 5. Based on the multimodal maps shown in Figure 5, associations of elements at these locations can be used to assist in determining P speciation. These five spectra are plotted in two different techniques: stacked and overlaid. Both plotting techniques aid in identification of distinct spectral features, such as the pre-edge feature at ca. 2150 eV. (b) Phosphorus K-edge µ-XANES (SM2 P2) from sample CGAp with two P standards: "P adsorbed to Mn" is P adsorbed to hydrous manganese oxide and "P adsorbed to Fe" is P adsorbed to ferrihydrite. CGAp is an agricultural soil, which was prepared as a petrographic thin section. SM2 P2 corresponds to the location labeled in Figure 5. These three spectra are plotted in two different techniques: stacked and overlaid. Both plotting techniques aid in identification of distinct spectral features, such as the pre-edge feature at ca. 2150 eV. The two standards aid in the fingerprinting technique, which is used to identify P species in the soil. From this plot, distinct pre-edge features can be seen at about 2150 eV.

in the LCF. This may again be a case of LCF fitting peak height rather than peak location as the main peak location for Phytate-Fe-Cop is 0.17 eV lower in energy than the main peak location for CGAp SM1 P1.

Using the fingerprinting by SFA, the pre-edge features and peak locations of the µ-XANES spectra collected at CGAp SM1 P1 and CGAp SM1 P2 were found to be nearly identical, indicating that these are similar species (Table 2, Figure S9). At CGAp SM1 P2, P is not co-located with S, but it is co-located with Al, Fe, and Mn. Some minor differences in the post-edge region and peak location may be due to the addition of P directly associated with Fe and a decrease in the contribution from Al.

The speciation determined by LCF found CGAp SM1 P2 to be P-Fe-Cop 15.3%, Phytate-Fe-Cop 10.5%, P-HMO-Sorb 36.7%, and P-Alumina-Sorb 36.3% (Table 3, Figure 4b), which are the same species determined for CGAp SM1 P1, but in different contributions. As in CGAp SM1 P1, there were notable differences in the speciation for CGAp SM1 P2 determined via LCF and the fingerprinting by SFA. Briefly, the peak locations of P-Fe-Cop and Phytate-Fe-Cop were not close to the peak location for CGAp SM1 P2 and no pre-edge feature doublet for Mn was determined using the fingerprinting by SFA.

With essentially the same peak location (2153.50 eV) as CGAp SM1 P1 (2153.49 eV) and CGAp SM1 P2 (2153.53 eV) and the same pre-edge feature, yet less intense, CGAp SM2 P3 is also a similar species (Figure S9, Table 2). CGAp SM2 P3 is co-located with Al, Fe, and Mn. CGAp SM1 P1 and CGAp SM1 P2 are also co-located with Fe, Mn, and

Al, strengthening evidence that these are all the same species. Much like the CGAp SM1 P1 and CGAp SM1 P2, there is a pre-edge that was fit with a peak doublet at the same locations as the P-Fe-Sorb doublet, but there is no Mn doublet under the pre-edge (Table 2). There is also no post-edge feature and organic P is not present. Therefore, CGAp SM2 P3 is P adsorbed to Al and Fe. The less intense pre-edge feature of CGAp SM2 P3 also had weak pre-edge peaks, so this sample has a lower contribution of P adsorbed to Fe and a higher contribution of P adsorbed to Al.

The LCF of CGAp SM2 P3 determined the P speciation to be Phytate-Fe-Cop 21.9%, P-HMO-Sorb 36.2%, and P-Boehmite-Sorb 42.2% (Table 3, Figure 4b). There is agreement between LCF and the fingerprinting by SFA with P adsorbed to Al (P-Boehmite-Sorb); however, the two analyses differed with what Fe-P species was included as well as the addition of Mn in the LCF. The fingerprinting by SFA determined that there is no contribution from organic P, and there is no Mn as there is no pre-edge doublet peak for Mn (Table 2). This is likely another case of LCF not being sensitive enough to distinguish between minute spectral differences in the P-Fe and P-Mn pre-edge. Fingerprinting by SFA, on the other hand, is sensitive enough to determine these minor differences in the pre-edge region.

The CGAp SM1 P3 spectrum is very different from the other spectra collected from this sample (Figures 5 and 6a and Figure S10). There is no pre-edge feature, and the low peak height indicates self-absorption or a crystalline species (Gamble et al., 2020). The main peak has both pre- and post-edge shoulders. The well-defined post-edge also has two "jagged" secondary peaks (at 2159.30 and 2171.20 eV). These sharp peaks indicate that CGAp SM1 P3 is possibly a crystalline P species. Also, the white line peak location is toward the lower energy range commonly seen for P white lines (Table 2) at 2153.29 eV. At CGAp SM1 P3, P is not co-located with S, but it is co-located with Al. Unfortunately, this point is right on the edge of the XFM map (Figure 5d) and appears to be out of bounds for the map so hard energy elemental co-location was not determined. Upon comparing the CGAp SM1 P3 spectra with other published standards, there is no clear match with other reference databases. The post-edge peak in CGAp SM1 P3 has similar features to pyromorphite (see Ingall et al., 2011); however, it lacks the necessary pre-edge features. Therefore, CGAp SM1 P3 is yet to be identified via fingerprinting by SFA.

The LCF of CGAp SM1 P3 determined the P speciation to be P-Alumina-Sorb 3.5%, Fluorapatite 11.7%, Monetite 49.6%, and ATP 31.5% (Table 3). The overall LCF fit was poor noticeably poor when comparing the fit spectrum with the data (Figure 4b), with the LCF fit of the post-edge region not lining up with the data (*R*-factor of 0.021). Therefore, it is very unlikely that the species determined via LCF are the species at CGAp SM1 P3.

CGAp SM2 P1 does not have a pre-edge feature; however, the spectrum has a well-defined post-edge region, which is indicative of a crystalline species (Figures 4 and 6a and Figure S10). The peak location is 2153.43 eV, which is over 0.14 eV higher in energy than CGAp SM1 P3, indicating that these are different species. The location of the main peak is close to that of P-Boehmite-Sorb (2153.46 eV) and P-Alumina-Sorb (2153.48 eV) as well as P-Fe-Sorb (2153.47 eV); however, P-Fe-Sorb was ruled out as CGAp SM2 P1 does not have a pre-edge feature (Table 2). The spectrum for CGAp SM2 P1 is not readily identifiable and does not match any published standards, similar to CGAp SM1 P3. CGAp SM2 P1 is co-located with Al on the TES μ-XRF map (Figure 5a, 5c) and Ca and Mn on the XFM map (Figure 5d). To discern this species, it is necessary to use the spectra, both tender and hard energy μ-XRF maps, and published standards to narrow down possibilities. With the current information, this is likely a crystalline P-Al species based on the location of the main peak and the observation that the crystalline standards (e.g., fluorapatite and monetite) have the most defined post-edge features.

The LCF of CGAp SM2 P1 found P speciation to be P-Alumina-Sorb 39.5%, Fluorapatite 10.6%, and Monetite 49.4% (Table 3). Here, both LCF and fingerprinting by SFA identified P-Alumina-Sorb to be a component. However, the LCF fit did not match the post edge region of the data, and the fit was poor with an *R*-factor of 0.01 (Table 3, Figure 4b). Therefore, the species identified during LCF do not describe CGAp SM2 P1 very well.

While CGAp SM2 P1 and CGAp SM1 P3 do not have distinguishing pre-edge features, in contrast, CGAp SM2 P2 (Figure 6b) has a pre-edge feature and a very sharp peak. The tall, sharp peak is an indicator for an adsorbed species. The pre-edge feature does not appear to be the same shape as any of the Fe standards (Figure 6b, Figure S1) and is more similar in shape to the P-HMO-Sorb (Figure 6b). The peak location for CGAp SM2 P2 (2153.58 eV) is closer to P-HMO-Sorb (2153.60 eV) and P-Fe-Cop (2153.62 eV) than P-Fe-Sorb (2153.45 eV). Using SFA, the pre-edge peaks were intense for the match with P-HMO-Sorb, with some contribution from P-Fe-Cop, but were not as intense, indicating this species is primarily P-HMO-Sorb with minor contribution from P-Fe-Cop. Given only the spectral data, CGAp SM2 P2 has the same line shape as the P adsorbed to the Mn standard. On the map, at CGAp SM2 P2, P is co-located with S, Ca, Mn, and Fe. The co-location with Mn adds further evidence that this is P adsorbed to Mn oxide. CGAp SM2 P2 appears to be located on or near a single large particle that contains elevated concentrations of S and Ca, and Mn exists as a small bright spot within the Ca background (XFM map, Figure 5d). With confidence, CGAp SM2 P2 is primarily P-HMO-Sorb with minor contribution from P-Fe-Cop. This is unexpected because, typically, P binds more strongly with Al and Fe in soil than Mn

due to the higher PZC of Al and Fe. However, P bound to HMO was found in the soil, so it is a unique observation. This is important because P-Mn species are not typically chosen for LCF. This point was also co-located with Mn, further proving that the unique pre-edge feature indicates direct associations of P with Mn. The LCF of CGAp SM2 P2 determined the P speciation to be P-Fe-Cop 13.6%, P-HMO-Sorb 67.6%, and Monetite 13% (Table 3). Here, the fingerprinting by SFA and LCF agree for the most part on the P species that comprise CGAp SM2 P2. Interestingly, both methods determined the P speciation to be primarily P-HMO-Sorb with a small amount of P-Fe-Cop. The only discrepancy is the addition of the Monetite standard in the LCF fit.

3.5 | Spectra interpretation and challenges

LCF is traditionally used to interpret XANES spectra of different P species in soils (e.g., Szerlag et al., 2022). However, this is common practice mainly with bulk XANES measurements, whereas here we present micro-focused (μ) XANES measurements. With μ-XANES, other issues can arise that prevent utilization of LCF as an appropriate analysis technique (Gamble et al., 2020). For this reason, we focus our approach on the fingerprinting by SFA technique (Table 2, Figures 4 and 5, and Figures S4, S7–S9) and then compared it with traditional LCF. Some of the reasons for this is because μ-XANES is particularly sensitive to differences in the size of the particle from which spectra are collected (i.e., "particle size effects") as well as self-absorption (also termed "over-absorption") due to localized high concentrations of the element of interest. Typically for bulk XAS data collection, self-absorption can be reduced by diluting the sample. However, this is not possible for micro-focused work where often single particles (i.e., tens of microns in size) are of interest. Therefore, due to the likelihood of these processes, the μ-XANES collected during this study are analyzed via the fingerprinting by SFA technique and then compared to traditional LCF. Particle size effects can occur with bulk beam but are more pronounced with micro-focused beam and can look similar to self-absorption. Therefore, any evidence of self-absorption may actually be due to particle size effects.

The two processes, however, are distinct. Self-absorption is caused by an abrupt change in sampling depth while scanning in energy (Lombi et al., 2006; Schefe et al., 2011). At energy prior to the white line the sampling depth is deeper; at the white line, an abrupt change to a lower sampling depth takes place. This occurs because at higher concentrations of the absorbing atom, a significant fraction of the incident beam is absorbed at a shallower sample depth than the beam penetration depth through the matrix alone. Spectra with self-absorption have an increase in intensity of pre-edge features and a dampening of post-edge features.

With the effects of particle size, more PO_4 tetrahedra are in closer proximity within larger particles of a concentrated phase, whereas in isolated phosphate tetrahedra (the smallest possible particle size), such as adsorbed species, the main peak is due to excitation of the P 1s electron to an available P 3p—O 2p energy level (Khare et al., 2007), and that destination is a discrete energy leading to a narrow tall peak. If there are more phosphate tetrahedra in close proximity, as particle size of a pure phosphate phase increases, then those available energy levels interact, forming a band-like energy level that is less discrete in energy. Thus, the XANES peak becomes broader and less tall, and appears similar to self-absorption. For example, mineral P species, like apatite, have more phosphate in close proximity. This causes μ-XANES spectra with a shortened and widened peak. This effect is important in the range from dilute or adsorbed isolated phosphate tetrahedra to nanoparticles to the sub-micrometer scale. In contrast, self-absorption is a function of the overall concentration of P in the beam footprint, independent of particle size until the particle size is large enough to create self-absorption. Self-absorption can still occur at nanoparticle size if there is sufficient concentration of nanoparticles in the beam footprint. Particle size effects and self-absorption do not affect the location of the white-line or other spectral features (Gamble et al., 2020). Therefore, fingerprinting by SFA overcomes the pitfalls of fitting spectra with traditional LCF exhibiting particle size effects and/or self-absorption by focusing on peak location, spectral feature presence/absence/shape and location rather than placing emphasis on white-line peak height and shape.

4 | ENVIRONMENTAL IMPLICATIONS AND CONCLUSION

The advanced TES completed at NSLS II beamline 8-BM allowed for high-resolution P speciation in US Mid-Atlantic agricultural soils with elevated levels of legacy P. The ~0.1 eV repeatable energy resolution enabled the capture of the pre-edge features of P adsorbed to iron (i.e., "P-Fe-Sorb") in detail, allowing us to see, and successful modeling to identify two-components in the pre-edge (Figures S3–S5). Findings of this work include spectroscopic examples of these features within the soil samples, various P hotspots, and hotspots with features resulting from phosphate interaction with Mn phases.

The overall observation during this study is that even at the micron scale, complex soil systems still contain multiple P species at a single location. This makes it difficult to completely match standards to soil components because the standards represent a single species, while in soil, the single species may not exist, or at least not at the micron scale. The investigation into the EFT thin section indicated P speciation in and around OM identified through S and P colocation, and S μ-XANES confirmed the presence of five different organic S

species. While P species identified in the CGAp soil includes Fe, many of these species also include Mn but lack S. The presence of S indicated organic P in EFT (Figure 2), and the absence of sulfur may indicate adsorption of inorganic P species to oxide surfaces. The P species identified in CGAp were primarily inorganic P adsorbed to Fe, Al, and Mn.

The data analysis for the μ-XANES was completed by two different methods: the fingerprinting by SFA and the more traditional LCF. The fingerprinting by SFA was used due to the limitations of LCF with micro-focused data. Micro-focused XANES is particularly subject to self-absorption and particle size effects, which makes it difficult to accurately fit the data via LCF due to the peak height dominating the fit and not considering key spectral features like peak position and pre-edge features. Many of the LCF did not accurately describe the μ-XANES spectra due to these issues. In several cases, the results obtained by the fingerprinting by SFA differed from LCF and therefore provided a more accurate evaluation of the P species.

The Hedley sequential extraction from Szerlag et al. (2022) found that CGAp had less labile P than EFT. The P species found in both soils in this study were not labile. The majority of the species found in the solid phase via μ-XANES in this study were P bound to Ca, Al, Fe, and Mn. These species are not labile. Understanding the P speciation at the micron scale, as we have done here, is essential because the species captured at the micron scale contribute to P solubility and therefore mobility. The bulk scale XANES is limited due to only fitting major species and the potential problem of "overfitting" (Beauchemin et al., 2003). Therefore, here we present a robust analysis of how the fingerprinting by SFA technique at the micron-scale can be used to identify potential trace phases of P, which can significantly contribute to P mobility.

AUTHOR CONTRIBUTIONS

Kathryn D. Szerlag: Conceptualization; formal analysis; investigation; project administration; visualization; writing—original draft. **Matthew G. Siebecker**: Investigation; writing—original draft. **Fatemeh Izaditame**: Writing—review and editing. **Paul Northrup**: Formal analysis; investigation; writing—review and editing. **Ryan Tappero**: Investigation; writing—review and editing. **Donald L. Sparks**: Conceptualization; funding acquisition; resources; supervision; writing—review and editing.

ACKNOWLEDGMENTS

This research was funded by USDA-NIFA (National Institute of Food and Agriculture), grant number 2017-67019-26333. This research used the TES and XFM beamlines of the National Synchrotron Light Source II, a U.S. Department of Energy (DOE) Office of Science User Facility operated by Brookhaven National Laboratory under Contract No. DE-SC0012704. Measurements were supported by the Tender Energy Microspectroscopy Consortium.

CONFLICT OF INTEREST STATEMENT

The authors declare no conflicts of interest.

ORCID

Kathryn D. Szerlag https://orcid.org/0000-0002-4162-5408
Matthew G. Siebecker https://orcid.org/0000-0002-1348-6543
Paul Northrup https://orcid.org/0000-0002-6547-1028

REFERENCES

Beauchemin, S., Hesterberg, D., & Beauchemin, M. (2002). Principal component analysis approach for modeling sulfur K-XANES spectra of humic acids. *Soil Science Society of America Journal*, *66*, 83–91. https://doi.org/10.2136/sssaj2002.8300

Beauchemin, S., Hesterberg, D., Chou, J., Beauchemin, M., Simard, R. R., & Sayers, D. E. (2003). Speciation of phosphorus in phosphorus-enriched agricultural soils using X-ray absorption near-edge structure spectroscopy and chemical fractionation. *Journal of Environmental Quality*, *32*, 1809–1819. https://doi.org/10.2134/jeq2003.1809

Boesch, D. F., Brinsfield, R. B., & Magnien, R. E. (2001). Chesapeake Bay eutrophication. *Journal of Environmental Quality*, *30*, 303–320. https://doi.org/10.2134/jeq2001.302303x

Brandes, J. A., Ingall, E., & Paterson, D. (2007). Characterization of minerals and organic phosphorus species in marine sediments using soft X-ray fluorescence spectromicroscopy. *Marine Chemistry*, *103*, 250–265. https://doi.org/10.1016/j.marchem.2006.09.004

Calvin, S. (2013). *XAFS for everyone*. CRC Press.

Einsiedl, F., Schäfer, T., & Northrup, P. (2007). Combined sulfur K-edge XANES spectroscopy and stable isotope analyses of fulvic acids and groundwater sulfate identify sulfur cycling in a karstic catchment area. *Chemical Geology*, *238*, 268–276. https://doi.org/10.1016/j.chemgeo.2006.11.014

Gamble, A. V., Northrup, P. A., & Sparks, D. L. (2020). Elucidation of soil phosphorus speciation in Mid-Atlantic soils using synchrotron-based microspectroscopic techniques. *Journal of Environmental Quality*, *49*, 184–193. https://doi.org/10.1002/jeq2.20027

Giannetta, B., Plaza, C., Siebecker, M. G., Aquilanti, G., Vischetti, C., Plaisier, J. R., Juanco, M., Sparks, D. L., & Zaccone, C. (2020). Iron speciation in organic matter fractions isolated from soils amended with biochar and organic fertilizers. *Environmental Science & Technology*, *54*(8), 5093–5101.

Gu, C., Dam, T., Hart, S. C., Turner, B. L., Chadwick, O. A., Berhe, A. A., Hu, Y., & Zhu, M. (2020). Quantifying uncertainties in sequential chemical extraction of soil phosphorus using XANES spectroscopy. *Environmental Science & Technology*, *54*(4), 2257–2267. https://doi.org/10.1021/acs.est.9b05278

Gustafsson, J. P., Braun, S., Tuyishime, J. R. M., Adediran, G. A., Warrinnier, R., & Hesterberg, D. (2020). A probabilistic approach to phosphorus speciation of soils using P K-edge XANES spectroscopy with linear combination fitting. *Soil Systems*, *4*(2), 26. https://doi.org/10.3390/soilsystems4020026

Hesterberg, D., McNulty, I., & Thieme, J. (2017). Speciation of soil phosphorus assessed by XANES spectroscopy at different spatial

scales. *Journal of Environmental Quality*, *46*, 1190–1197. https://doi.org/10.2134/jeq2016.11.0431

Hesterberg, D., Zhou, W., Hutchison, K. J., Beauchemin, S., & Sayers, D. (1999). XAFS study of adsorbed and mineral forms of phosphate. *Journal of Synchrotron Radiation*, *6*, 636–638. https://doi.org/10.1107/S0909049599000370

Ingall, E. D., Brandes, J. A., Diaz, J. M., De Jonge, M. D., Paterson, D., McNulty, I., Elliott Crawford, W., & Northrup, P. (2011). Phosphorus K-edge XANES spectroscopy of mineral standards. *Journal of Synchrotron Radiation*, *18*(2), 189–197. https://doi.org/10.1107/S0909049510045322

Jarvie, H. P., Sharpley, A. N., Spears, B., Buda, A. R., May, L., & Kleinman, P. J. A. (2013). Water quality remediation faces unprecedented challenges from "legacy phosphorus." *Environmental Science & Technology*, *47*, 8997–8998.

Khare, N., Hesterberg, D., Beauchemin, S., & Wang, S. (2004). XANES determination of adsorbed phosphate distribution between ferrihydriteand boehmite in mixtures. *Soil Science Society of America Journal*, *68*, 460–469. https://doi.org/10.2136/sssaj2004.4600

Khare, N., Martin, J. D., & Hesterberg, D. (2007). Phosphate bonding configuration on ferrihydrite based on molecular orbital calculations and XANES fingerprinting. *Geochimica et Cosmochimica Acta*, *71*(18), 4405–4415.

Kleinman, P. J. A., Sharpley, A., Buda, A., McDowell, R., & Allen, A. (2011). Soil controls of phosphorus in runoff: Management barriers and opportunities. *Canadian Journal of Soil Science*, *91*, 329–338.

Kruse, J., & Leinweber, P. (2008). Phosphorus in sequentially extracted fen peat soils: A K-edge X-ray absorption near-edge structure (XANES) spectroscopy study. *Journal of Plant Nutrition & Soil Science*, *171*, 613–620. https://doi.org/10.1002/jpln.200700237

Lombi, E., Scheckel, K. G., Armstrong, R. D., Forrester, S., Cutler, J. N., & Paterson, D. (2006). Speciation and distribution of phosphorus in a fertilized soil: A synchrotron-based investigation. *Soil Science Society of America Journal*, *70*, 2038–2048. https://doi.org/10.2136/sssaj2006.0051

McDowell, R. W., Sharpley, A. N., & Chalmers, A. T. (2002). Land use and flow regime effects on phosphorus chemical dynamics in the fluvial sediment of the Winooski River, Vermont. *Ecological Engineering*, *18*, 477–487. https://doi.org/10.1016/S0925-8574(01)00108-2

Newville, M. (2013). Larch: An analysis package for XAFS and related spectroscopies. *Journal of Physics: Conference Series*, *430*, 012007. https://dx.doi.org/10.1088/1742-6596/430/1/012007

Northrup, P. (2019). The TES beamline (8-BM) at NSLS-II: Tender-energy spatially resolved X-ray absorption spectroscopy and X-ray fluorescence imaging. *Journal of Synchrotron Radiation*, *26*, 2064–2074. https://doi.org/10.1107/S1600577519012761

Northrup, P., Tappero, R., Glotch, T., Flynn, G. J., Yesiltas, M., Kebukawa, Y., Flores, L., Gemma, M., & Piccione, G. (2024). Chemistry in retrieved Ryugu asteroid samples revealed by non-invasive X-ray microanalyses: Pink-beam fluorescence CT and tender-energy absorption spectroscopy. *Geosciences*, *14*(4), 111.

Peak, D., Sims, J. T., & Sparks, D. L. (2002). Solid-state speciation of natural and alum-amended poultry litter using XANES spectroscopy. *Environmental Science & Technology*, *36*, 4253–4261. https://doi.org/10.1021/es025660d

Prietzel, J., Botzaki, A., Tyufekchieva, N., Brettholle, M., Thieme, J., & Klysubun, W. (2011). Sulfur speciation in soil by S K-edge XANES spectroscopy: Comparison of spectral deconvolution and linear combination fitting. *Environmental Science and Technology*, *45*(7), 2878–2886. https://doi.org/10.1021/es102180a

Prietzel, J., Harrington, G., Häusler, W., Heister, K., Werner, F., & Klysubun, W. (2016). Reference spectra of important adsorbed organic and inorganic phosphate binding forms for soil P speciation using synchrotron-based K-edge XANES spectroscopy. *Journal of Synchrotron Radiation*, *23*, 532–544. https://doi.org/10.1107/S1600577515023085

Qin, Z., & Shober, A. L. (2018). The challenges of managing legacy phosphorus losses from manure-impacted agricultural soils. *Current Pollution Reports*, *4*, 265–276. https://doi.org/10.1007/s40726-018-0100-1

Ravel, B., & Newville, M. (2005). Athena, Artemis, Hephaestus: Data analysis for X-ray absorption spectroscopy using IFEFFIT. *Journal of Synchrotron Radiation*, *12*, 537–541. https://doi.org/10.1107/S0909049505012719

Santoro, V., Martin, M., Persson, P., Lerda, C., Said-Pullicino, D., Magnacca, G., & Celi, L. (2019). Inorganic and organic P retention by coprecipitation during ferrous iron oxidation. *Geoderma*, *348*, 168–180. https://doi.org/10.1016/j.geoderma.2019.04.004

Sato, S., Solomon, D., Hyland, C., Ketterings, Q. M., & Lehmann, J. (2005). Phosphorus speciation in manure and manure-amended soils using XANES spectroscopy. *Environmental Science & Technology*, *39*, 7485–7491.

Schefe, C. R., Kappen, P., & Pigram, P. J. (2011). Carboxylic acids affect sorption and micro-scale distribution of phosphorus in an acidic soil. *Soil Science Society of America Journal*, *75*, 35–44. https://doi.org/10.2136/sssaj2010.0068

Sharpley, A. N., Kleinman, P. J. A., Flaten, D. N., & Buda, A. R. (2011). Critical source area management of agricultural phosphorus: Experiences, challenges and opportunities. *Water Science and Technology*, *64*, 945–952. https://doi.org/10.2166/wst.2011.712

Shober, A. L., Hesterberg, D. L., Sims, J. T., & Gardner, S. (2006). Characterization of phosphorus species in biosolids and manures using XANES spectroscopy. *Journal of Environmental Quality*, *35*, 1983–1993. https://doi.org/10.2134/jeq2006.0100

Shober, A. L., & Sims, J. T. (2016). *Phosphorus management strategies for Delaware's agricultural soils: The phosphorus site index*. UD Cooperative Extension. https://www.udel.edu/academics/colleges/canr/cooperative-extension/fact-sheets/phosphorus-management-strategies-for-delawares-agricultural-soils-the-phosphorus-site-index/#:~:text=Based%20on%20Delaware%20state%20law,%2D1%20Mehlich%201%20P)

Siebecker, M. G., Chaney, R. L., & Sparks, D. L. (2017). Nickel speciation in several serpentine (ultramafic) topsoils via bulk synchrotron-based techniques. *Geoderma*, *298*, 35–45. https://doi.org/10.1016/j.geoderma.2017.03.008

Siebecker, M. G., Chaney, R. L., & Sparks, D. L. (2018). Natural speciation of nickel at the micrometer scale in serpentine (ultramafic) topsoils using microfocused X-ray fluorescence, diffraction, and absorption. *Geochemical Transactions*, *19*, 1–16.

Soper, D. (2020). *Free statistics calculators*. https://www.danielsoper.com/statcalc/calculator.aspx?id=37

Szerlag, K. D., Elavarthi, M., Siebecker, M. G., Gu, C., McCrone, C., & Sparks, D. L. (2022). Systematic study of legacy phosphorus (P) desorption mechanisms in high-P agricultural soils. *Minerals*, *12*(4), 458. https://doi.org/10.3390/min12040458

Toor, G. S., Hunger, S., Peak, J. D., Sims, J. T., & Sparks, D. L. (2006). Advances in the characterization of phosphorus in organic wastes:

Environmental and agronomic applications. *Advances in Agronomy*, *89*, 1–72. https://doi.org/10.1016/S0065-2113(05)89001-7

Toor, G. S., Peak, J. D., & Sims, J. T. (2005). Phosphorus speciation in broiler litter and turkey manure produced from modified diets. *Journal of Environmental Quality*, *697*, 687–697. https://doi.org/10.2134/jeq2005.0687

Tully, K. L., Gedan, K., Epanchin-Niell, R., Strong, A., Bernhardt, E. S., BenDor, T., Mitchell, M., Kominoski, J., Jordan, T. E., Neubauer, S. C., & Weston, N. B. (2019). The invisible flood: The chemistry, ecology, and social implications of coastal saltwater intrusion. *Bioscience*, *69*, 368–378. https://doi.org/10.1093/biosci/biz027

Tully, K. L., Weissman, D., Wyner, W. J., Miller, J., & Jordan, T. J. B. (2019). Soils in transition: Saltwater intrusion alters soil chemistry in agricultural fields. *Biogeochemistry*, *142*, 339–356. https://doi.org/10.1007/s10533-019-00538-9

Xia, K., Weesner, F., Bleam, W. F., Bloom, P. R., Skyllberg, U. L., & Helmke, P. A. (1998). XANES studies of oxidation states of sulfur in aquatic and humic substances. *Soil Science Society of America Journal*, *62*, 1240–1246. https://doi.org/10.2136/sssaj1998.03615995006200050014x

Yamaguchi, N., Ohkura, T., Hikono, A., Hashimoto, Y., Suda, A., Yamamoto, T., Ando, K., Kasuya, M., Northrup, P., Wang, S.-L., & Hesterberg, D. (2021). Microscale heterogeneous distribution and speciation of phosphorus in Soils amended with mineral fertilizer and cattle manure compost. *Minerals*, *11*(2), 121. https://doi.org/10.3390/min11020121

Zhang, J., Sun, Y., Cao, Z., Li, C., Zhu, M., & Zhu, P. (2022). Long-term fertilization impacts on soil phosphorus forms using XANES and NMR spectroscopy. *Archives of Agronomy and Soil Science*, *69*(8), 1266–1281. https://doi.org/10.1080/03650340.2022.2082417

SUPPORTING INFORMATION

Additional supporting information can be found online in the Supporting Information section at the end of this article.

How to cite this article: Szerlag, K. D., Siebecker, M. G., Izaditame, F., Northrup, P., Tappero, R., & Sparks, D. L. (2024). Multimodal, microspectroscopic speciation of legacy phosphorus in two US Mid-Atlantic agricultural soils. *Soil Science Society of America Journal*, 1–21. https://doi.org/10.1002/saj2.20765